HERON is jointly edited by:
STEVIN-LABORATORY of the faculty of Civil Engineering, Delft University of Technology, Delft, The Netherlands
and
TNO-INSTITUTE FOR BUILDING MATERIALS AND STRUCTURES.
Rijswijk (ZH), The Netherlands
HERON contains contributions based mainly on research work performed in these laboratories on strength of materials, structures and materials science.

ISSN 0046-7316

Secretary:
G. J. van Alphen
Stevinweg 1
P.O. Box 5048
2600 GA Delft, The Netherlands
Tel. 0031-15-785919
Telex 38070 BITHD

HERON vol. 34 1989 no. 4

Contents

COMPOSITE STEEL AND CONCRETE BEAMS WITH PARTIAL SHEAR CONNECTION

J. W. B. Stark
TNO Institute for Building Materials and Structures

Centrum Staal

Staalbouwkundig Genootschap

Civieltechnisch Centrum Uitvoering Research en Regelgeving

Preface

This publication presents the theoretical and experimental results of a research programme on composite beams with partial shear connection in buildings. It covers both simply supported and continuous beams. The results provide information on the influence of the number of shear connectors on the behaviour of composite beams. It is clearly illustrated that the deformation capacity of connectors has a significant influence on the resistance of composite beams with partial shear connection. Simplified methods for ductile and non-ductile shear connectors suitable for the daily engineering practice are derived from the partial connection theory.

Previously the work was published in Dutch in two reports including background information on the Dutch Recommendations on composite constructions. In view of the actual discussion on this topic in the drafting of Eurocode 4, it was decided to publish in English as well.

The research was carried out at the TNO Institute for Building Materials and Structures (TNO-IBBC). The project was supervised by a joint committee from the Dutch Centre for Civil Engineering Research and Codes (CUR) and the Dutch Steel Constructional Association (SG), which both supported the project financially. The research on simply supported beams was conducted by prof. ir. J. W. B. Stark. The research on continuous beams was carried out by ir. H. S. Buitenkamp, ir. J. G. J. Alma and prof. ir. J. W. B. Stark.

Financial support for this publication was provided by the Dutch Steel Information Centre (Centrum Staal), the Dutch Steel Constructional Association (Staalbouwkundig Genootschap) and the Dutch Centre for Civil Engineering Research and Codes (Stichting Civieltechnisch Centrum Uitvoering Research en Regelgeving). The main activities of these Dutch centres are in co-ordinating research and development projects, encouraging the spread and increase of knowledge and publishing recommendations, specifications and codes.

Acknowledgement is due to Mrs. D. van Hove for her help in summarizing the material from the original reports and to Mrs. A. Visser for the translation into English.

Composite steel and concrete beams with partial shear connection

1 Introduction

1.1 *Definition*

The behaviour of a composite steel and concrete beam is characterized by the presence of a shear connection between the concrete slab and the steel beam. A full shear connection is formed when the shear connection is so strong that the ultimate load is determined by the maximum moments of resistance. The maximum load is reached when the optimum stress distribution occurs in the cross-sections of maximum bending moment (Fig. 1, cross-section II). The application of more shear connectors cannot result in a larger maximum load, as the maximum moments are normative.

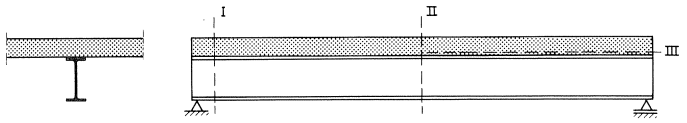

Fig. 1. Cross-sections that may be critical for failure.

However, when fewer shear connectors are used, this will result in a smaller ultimate load, dependent on the number of shear connectors applied (Fig. 1, cross-section III). The shear connection is then defined as a partial shear connection. The limit is reached when no shear connectors at all are used. In that case the contribution of the concrete flange can usually be neglected. Then the ultimate load equals the ultimate load of the steel beam. Fig. 2 qualitatively shows the relation between the ultimate load and the

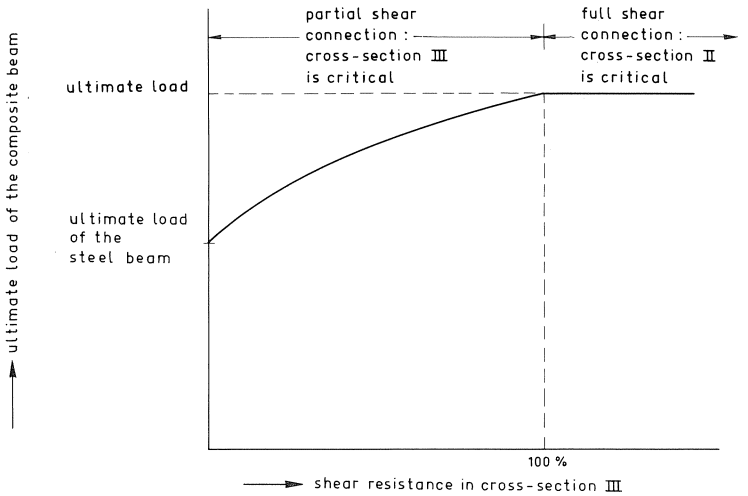

Fig. 2. Qualitative relation between the ultimate load and the longitudinal shear resistance.

strength of the shear connection, where 100% corresponds with the shear resistance in case of a full shear connection.
The concepts full and partial *shear connection* are related to the *strength* of the longitudinal shear connection. The concepts complete and partial *interaction* only relate to the *stiffness* of the connection between the concrete slab and the steel beam.
When slip between the steel and the concrete is completely prevented by the connection, the interaction is said to be complete. However, most shear connectors have to undergo some deformation before they can supply any force. In that case the interaction is essentially partial. This difference is illustrated in Fig. 3. Fig. 4 shows the influence of the longitudinal slip on the form of a M-$\varkappa$ diagram.

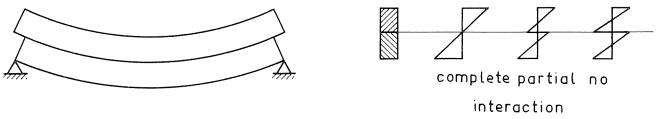

Fig. 3. Two beams showing different degrees of interaction.

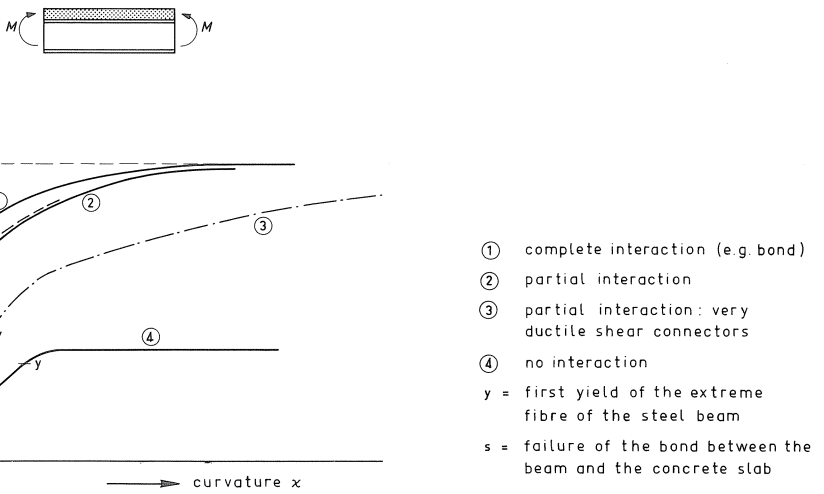

Fig. 4. Influence of slip on a M-$\varkappa$ diagram.

1.2 *Composite steel and concrete beams with partial shear connection*

1.2.1 Motivation for the application of partial shear connection

The application of partial shear connection is of interest in those structures in which cooperation between the steel section and the concrete slab need not be fully exploited to get sufficient resistance. This may occur in the following cases.

a. When the concrete slab is not propped, the dimensions of the steel beam may be determined by the load during laying of the concrete. In that case it is not economical to determine the number of stud connectors from the full plastic moment of resistance of the composite cross-section, because the composite beams will then be too strong for the load applied after the concrete has hardened.
b. According to the deflection limitations the stiffness of the composite beam can be critical for the dimensions of the beam.
c. For economical and technical reasons a designer may choose a larger steel section with fewer shear connectors instead of a minimum steel section with a relatively large number of shear connectors.

1.2.2 Qualitative description of the behaviour

Beams with partial shear connection will fail as a result of failure of the shear connection. The moments of resistance of the critical cross-sections have to be determined in order to determine the ultimate load.
The ultimate load depends on:
a. the number of shear connectors, which determines the resistance of the shear connection;
b. the type of shear connectors, which determines the deformation characteristics of the shear connection.

Fig. 5 shows the difference in behaviour of ductile shear connectors and absolutely rigid non-ductile shear connectors. With regard to the stress distribution at failure, the compressive force in the concrete and the resulting tensile force in the steel respectively, have to be equal to the total shear force that can be transferred by the shear connectors longitudinally (= shear resistance). In principle various stress distributions may occur.
When ductile shear connectors are applied, slip may occur at the interface between the steel beam and the concrete slab. Once the ultimate load of a shear connector is reached, the load remains constant with further slip. Then stress distributions occur in which the neutral axes in the concrete slab and the steel beam no longer coincide. On the basis of Kist's hypothesis (2nd law of Prager), a stress distribution will occur at failure that leads to the maximum moment of resistance corresponding to the applied number of shear connectors (provided the deformation capacity is sufficient). This moment of resistance can be determined on the basis of equilibrium.
When absolutely rigid non-ductile shear connectors are applied, fracture will occur when the ultimate load of a shear connector is reached without any slip and subsequently the shear resistance will suddenly drop to zero. So in theory no slip is possible before failure, which means that the strain distribution and consequently the stress distribution are fixed. The neutral axes in the steel beam and the concrete slab coincide. As soon as, under an increasing load, the longitudinal shear force on the heaviest loaded shear connector becomes equal to its shear resistance, the ultimate load is reached. Unless the distribution of the shear connectors coincides with the distribution of the longitudinal shear force, the total longitudinal shear resistance at failure is not equal to

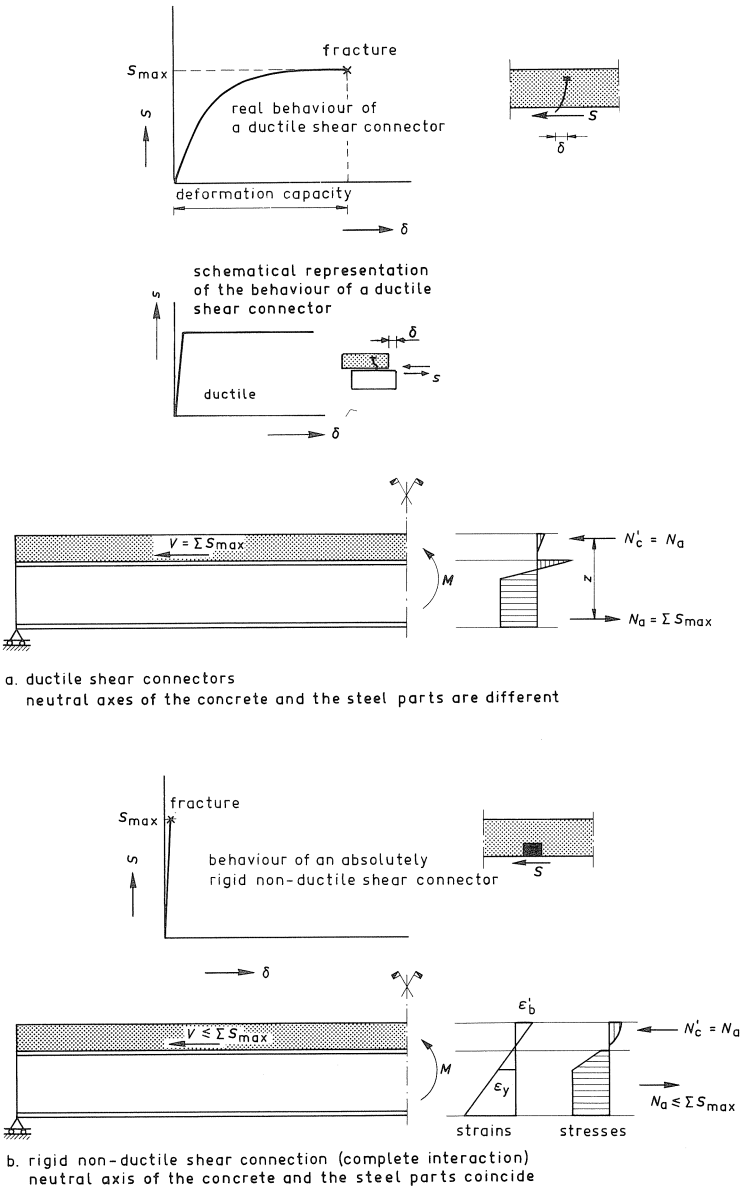

Fig. 5. The influence of the deformation capacity of shear connectors on the strain and the stress distribution in case of a partial shear connection.

the sum of the shear resistances of the shear connectors. In reality the so-called rigid shear connectors that are applied in practice (e.g. block connectors), do have some deformation capacity, so that some redistribution of the forces on the shear connectors may occur.

Fig. 6 qualitatively shows the relation between the moment of resistance and the

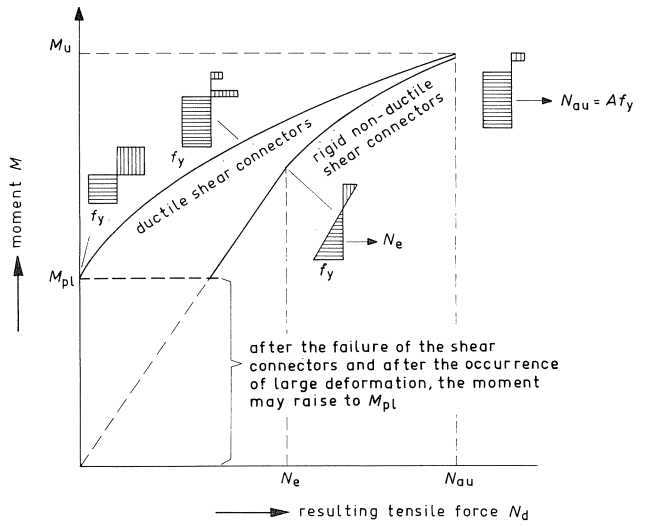

Fig. 6. Qualitative relation between the moment of resistance and the tensile force in the steel beam (=longitudinal shear force) at failure.

resulting tensile force in the steel beam at failure. So, these lines indicate the moments of resistance for various beams, each with a different number of shear connectors. The tensile force N_{au}, which will occur at failure, is determined by the number of shear connectors. For some specific cases the stress distribution over the cross-section at failure is shown in Fig. 6. In case of rigid non-ductile shear connectors, failure of the shear connection has been taken as a criterion. When very few shear connectors are applied the moment of resistance will be smaller than the plastic moment M_{pl} of the steel beam. After failure of the shear connection, large deformations occur due to a sudden drop in stiffness. However, after this sudden increase of deformation, it will theoretically be possible to raise the bending moment to M_{pl} (dashed line in Fig. 6). This region has no practical use, because application of a composite structure in that region does not offer any advantages.

The relation shown in Fig. 6 for rigid non-ductile shear connectors, is influenced by preloading of the steel beam and by internal stresses, for example caused by shrinkage and creep of the concrete. This means that in case of a *partial* shear connection and application of very *rigid* non-ductile shear connectors, the ultimate load is indeed influenced by these factors. This contrary to beams with full shear connection and beams with partial shear connection with ductile shear connectors. This is caused by the fact that the ultimate load is determined by a part of the structure that does not meet with the requirements of ideal plastic behaviour of the materials (the rigid connection with limited deformation capacity).

As an example the effect of pre-loading of the steel beam is illustrated in Fig. 7. The design curves for rigid non-ductile shear connectors will be different for propped and unpropped constructions, which is not the case when ductile shear connectors are used (see Fig. 35). This matter will be elaborated in chapter 3.

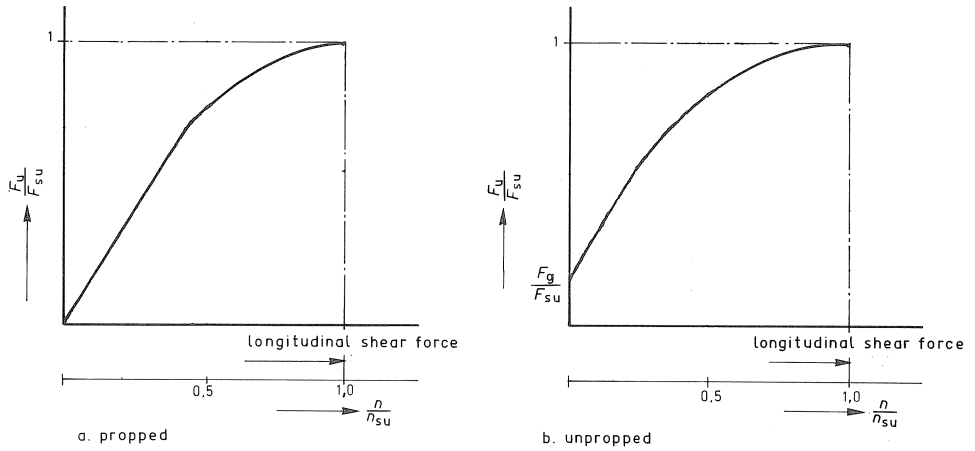

Fig. 7. Relation between the load and the longitudinal shear force i.e. the degree of shear connection, when rigid non-ductile shear connectors are applied.

2 The resistance of beams with full shear connection

2.1 *Moment of resistance of simply supported beams*

2.1.1 Elasto-plastic method

The ultimate load of a simply supported beam is determined by the moment of resistance of the critical cross-section. The determination of the moment of resistance of a cross-section is based on the following assumptions:

a. the shear connectors are able to transfer the forces occurring at failure between the steel and the concrete (full shear connection);
b. no slip occurs between the steel and the concrete;
c. tension stresses in the concrete are neglected;
d. the strains caused by bending are directly proportional to the distance from the neutral axis, in other words plane cross-sections remain plane after bending, even at failure;
e. the relation between the stress σ_a and the strain ε_a of steel is schematically represented by the bi-linear diagram shown in Fig. 8a;
f. the relation between the stress and the strain of the concrete is schematically represented by the simplified bi-linear diagram shown in Fig. 8b.

Based on these assumptions two cases can be distinguished:

a. the neutral axis is situated in the concrete slab (Fig. 9a);
b. the neutral axis is situated in the steel beam (Fig. 9b).

Fig. 9 shows that in case a_1 the calculation of the moment of resistance is simple. In the other cases the calculations are laborious. Therefore, a simplified method, applicable for all cases, will be described in the next paragraph.

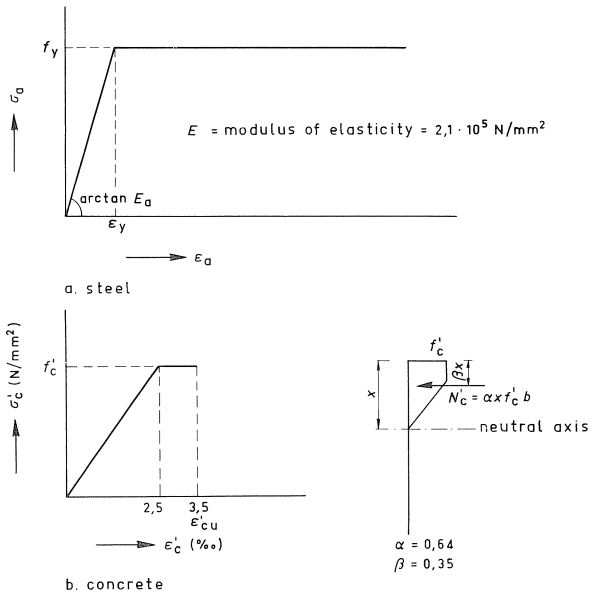

Fig. 8. Schematical representations of stress-strain diagrams of steel and concrete.

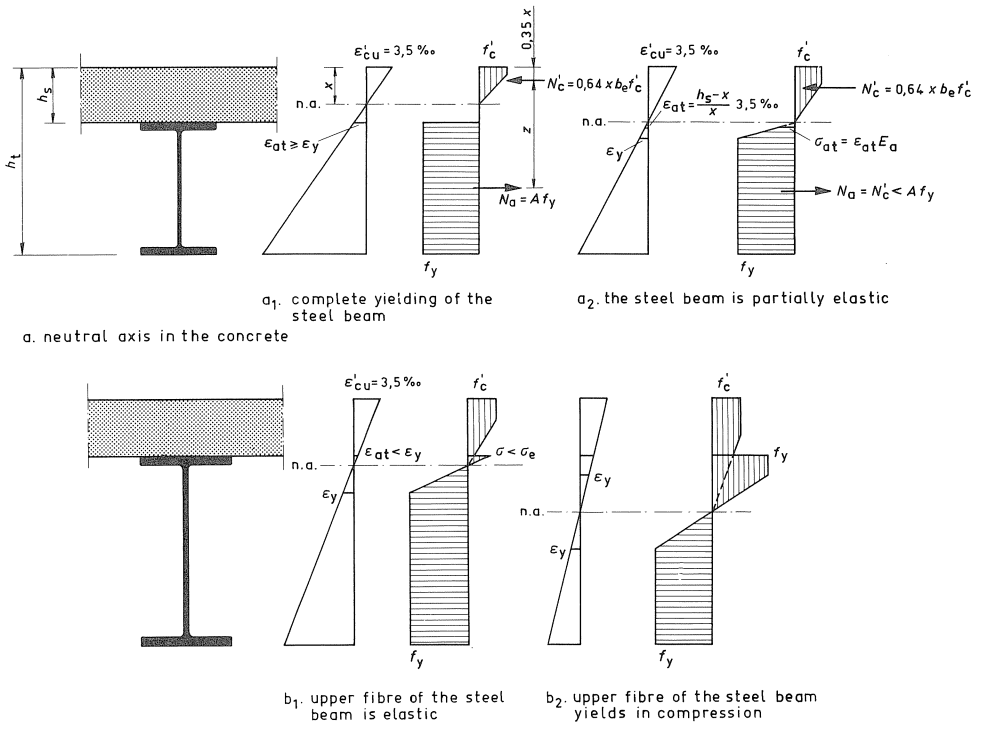

Fig. 9. Possible strain-stress distributions at failure.

2.1.2 Plastic method

The assumptions for the calculation of the moment of resistance are the same as those used in the elasto-plastic method (see 2.1.1), with the exception of the idealization of the stress-strain diagrams of steel and concrete. Both materials are assumed to behave as ideal plastic materials. So the strains are not limited. This is a usual assumption for structural steel, which is also used, for example, in the calculation of the plastic moment of a steel section. The idealized diagram of steel is shown in Fig. 10a.
The deviation between the real and the idealized diagram is much larger for concrete than for steel. If the maximum stress of concrete is assumed to have the same value as the value in the diagram in Fig. 8, the application of the idealized diagram will of course lead to an unconservative approximation of the moment of resistance. In practice the difference has appeared to be not very large. However, to be on the safe side, the design strength of concrete in the idealized diagram is assumed to have a reduced value kf'_c. The thus idealized σ-ε diagram is shown in Fig. 10b.

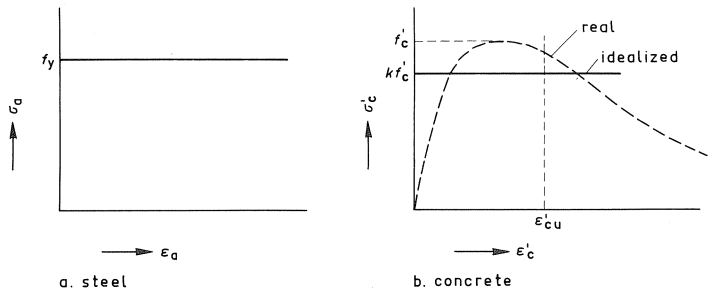

Fig. 10. Idealized σ-ε diagrams used in the plastic method.

Application of these assumptions leads to stress distributions as shown in the Figs. 11 and 12. Of course the calculation of the moment of resistance M_u is dependent on the position of the neutral axis. The position of the neutral axis is determined by the rela-

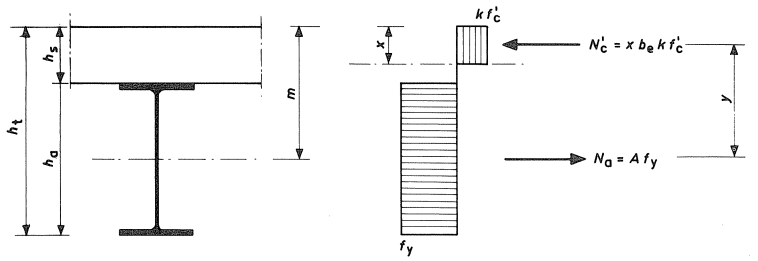

$$M_u = N_a z = Af_y(m - 0.5x)$$

$$M_u = Af_y\left(m - \frac{Af_y}{2b_e kf'_c}\right) \tag{2.1}$$

Fig. 11. Plastic stress distribution with the neutral axis situated in the concrete slab.

tion between the cross-section of the concrete slab and the cross-section of the steel beam.

Again two cases can be distinguished:
a. the neutral axis is situated in the concrete slab (Fig. 11);
b. the neutral axis is situated in the steel beam (Fig. 12).

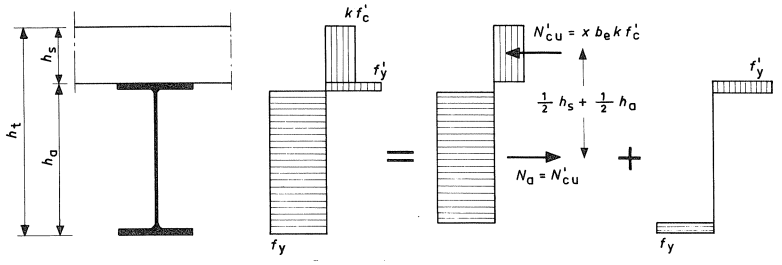

$$M_u = N'_{c,max} z + M_{pl,red} = N'_{c,max} 0.5 h_t + M_{pl,red}$$
$$M_u = 0.5 h_t h_s b_e k f'_c + M_{pl,red} \qquad (2.2)$$

Fig. 12. Plastic stress distribution with the neutral axis situated in the steel beam.

According to [4], the plastic moment reduced by a normal force for standard European rolled I or H steel sections, can be approximated by:

$$M_{pl,red} = 1.11 M_{pl} \left(1 - \frac{N'_{c,max}}{A f_y}\right) \qquad (2.3)$$

In this study the expression used in the Dutch Standard [6] is used. This means that $M_{pl,red}$ is calculated according to (2.4) when $N'_{c,max} > 0.15 A f_y$.

$$M_{pl,red} = 1.18 M_{pl} \left(1 - \frac{N'_{c,max}}{A f_y}\right) \qquad (2.4)$$

The moments of resistance, obtained by using the elasto-plastic method described in 2.1.1 and the plastic method respectively, will differ. Therefore a parameter study, described in [1], was carried out for comparison. The results of this study lead to the following conclusions:

- Within the variation of the parameters the largest difference between the moments of resistance according to the elasto-plastic method and those according to the plastic method, with $k = 1$, is about 6%.
  The largest difference between the elasto-plastic method and the plastic method with $k = 1$ was found for the stress distributions as shown in a2 and b1 of Fig. 9, i.e. when the neutral axis is close to the top of the steel beam. The differences in the cases a1 and b2 are small.
- It may be expected that the plastic method with $k = 0.8$ leads to a safe value for the

moment of resistance. This is only valid if the upper flange of the steel section has the same, or a smaller cross-section than the lower flange, which will usually be the case.

2.2 *Ultimate load of continuous beams*

The elastic moment distribution in continuous beams is not solely determined by equilibrium conditions, but also by compatibility conditions. When somewhere in the beam the yield strength is exceeded, a redistribution of the moments will occur. The moment distribution at failure is not only determined by the equilibrium condition, but also by the "mechanism" condition. The failure mechanism contains more than one plastic hinge. To allow for the redistribution of moments, the primary formed plastic hinges need to have sufficient rotation capacity. Because of these requirements regarding the rotation capacity, the scope of application for the plastic design is more restricted for continuous beams than for simply supported beams.

To determine the ultimate load of continuous beams with the plastic design method, no deformation requirements are needed. The ultimate load follows from the equilibrium of the statically determinate system at failure. In theory internal forces, for example caused by shrinkage and creep of concrete, pre-loading of the steel beam in the construction phase or subsidence of supports, have no influence on the plastic ultimate load. Also the plastic ultimate load of a continuous beam is, theoretically, not influenced by the stiffness of adjacent spans or by the stiffness of beam-to-column connections. Of course these factors do influence the deflections. It is possible that the deflection becomes so extreme, even before the plastic ultimate load is reached, that the plastic ultimate load no longer has any practical relevance. This implies further restrictions for the application of the plastic hinge theory.

The basic principles of the plastic design method for a beam over three supports are schematically represented in Fig. 13.

The calculation of the sagging moment of resistance M_{fu} is based on the same stress distribution over the cross-section as discussed in 2.1.2. The stress distributions over the cross-sections and the equations for the calculation of M_{fu} are given in the Figs. 11 and 12.

Analogous to the calculation of the sagging moment of resistance the calculation of the hogging moment of resistance M_{su} is based on the following assumptions (Fig. 14):

a. tension stresses in the concrete are neglected;
b. the reinforcement is yielding, so at failure the tensile force in the reinforcement is equal to $N_s = A_s f_{sy}$;
c. all fibers of the steel section are yielding either in compression or tension; from the equilibrium follows that the compressive force in the steel section is equal to $N'_{au} = N_s = A_s f_{sy}$; in addition the steel section is able to resist the plastic moment, reduced by the axial force, $M_{pl,red}$;
d. for the time being the possible influence of the vertical shear force on $M_{pl,red}$ is not taken into account.

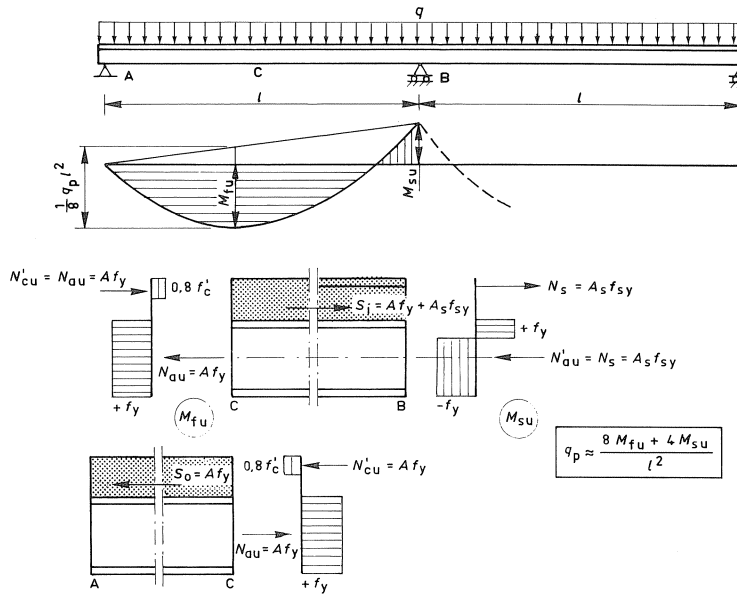

Fig. 13. Application of the plastic design method.

Fig. 14 shows a design method for the hogging moment of resistance M_{su} for a rolled I section without influence of the vertical shear force. The determination of the reduced moment $M_{pl,red}$ is discussed in paragraph 2.1.2.

$$M_{su} = N_s y + M_{pl,red} \tag{2.3}$$

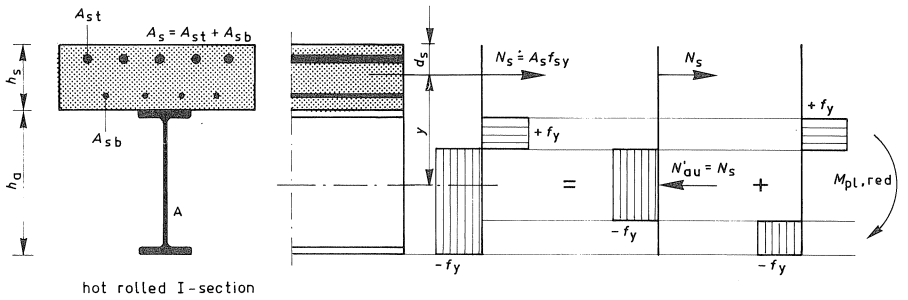

Fig. 14. Determination of the hogging moment of resistance M_{su}.

3 The resistance of beams with partial shear connection

3.1 *Moment of resistance of simply supported beams*

3.1.1 Beams with ideal ductile shear connectors

Based on the behaviour described in 1.2, a calculation method has been developed for beams with partial shear connection and ideal ductile shear connectors. When the

shear connectors have sufficient deformation capacity, the stress distribution in the critical cross-section will be such that the tensile force in the steel beam is equal to the sum of the resistances of the shear connectors (ΣS_u) and in addition the largest possible moment can be transferred.
The stress-strain diagrams of steel and concrete are idealised as shown in Fig. 10. The design strength of concrete is reduced to $0.8f'_c (k = 0.8)$, just as in beams with full shear connections.
Based on these assumptions the stress distribution at failure will be as shown in Fig. 15.

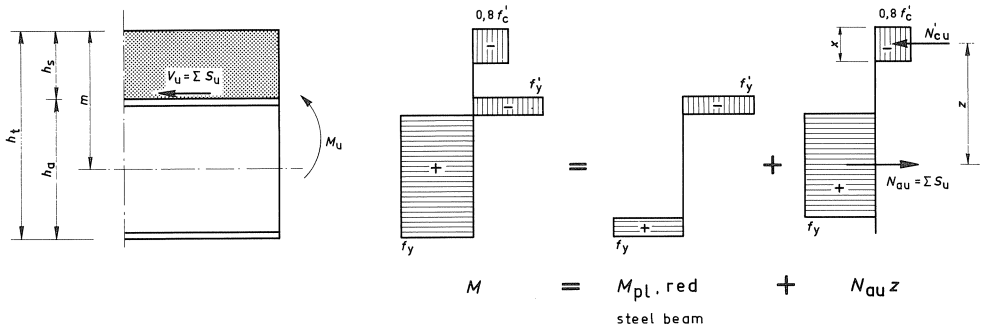

Fig. 15. Stress distribution if the shear connection is partial.

When a hot-rolled I section is used, the calculation may be simplified by splitting the moment of resistance into two parts as shown in Fig. 15 (compare Fig. 12). Equivalent to the derivation of equation (2.2) both parts of the moment can be calculated as follows:

- The part of the moment supplied by the normal forces in the steel beam and the concrete slab is:

$$M_{ul} = N_{au} z = N_{au}(m - 0.5x)$$

Where:

$$N_{au} = N'_{cu} = \Sigma S_u$$

$$x = \frac{\Sigma S_u}{0.8 b_e f'_c}$$

Therefore:

$$M_{ul} = \Sigma S_u (m - 0.5x)$$

- The part of the moment additionally supplied by the steel section (= reduced plastic moment) can be approximated for standard rolled European I or H sections by (also see 2.1.2):

$$M_{u2} = M_{pl,red} = 1.18M_{pl}\left(1 - \frac{N}{Af_y}\right)$$

Where:

$$N = N_{au} = \Sigma S_u$$

Therefore:

$$M_{u2} = 1.18M_{pl}\left(1 - \frac{\Sigma S_u}{Af_y}\right)$$

When the number of shear connectors and the design resistance of a shear connector are known (and so ΣS_u), the moment of resistance can be determined with the equation:

$$M_u = M_{ul} + M_{u2}$$

$$M_u = 1.18M_{pl}\left(1 - \frac{\Sigma S_u}{Af_y}\right) + \Sigma S_u(m - 0.5x) \qquad (3.1)$$

Fig. 16 shows the calculated relation between the ultimate load and the degree of shear connection according to equation (3.1) for the small-scale beams that are described in more detail in chapter 4. The values of the ultimate load that were found in the tests are plotted in the figure. In all tests this equation appeared to result in a safe value of the ultimate load.

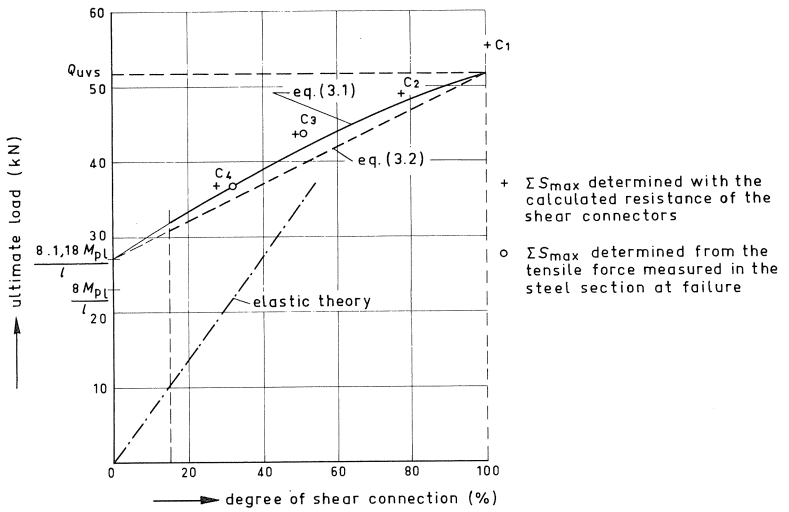

Fig. 16. Relation between the ultimate load and the percentage of ductile shear connectors for simply supported beams with a uniformly distributed load.

Simplified method

Assume that the height x of the compression zone in the concrete slab is known. A safe value is obtained if x is always taken as the value determined for full shear connections (see equations 2.1), because when ΣS_u decreases, N'_{cu} also decreases and so does the height of the compression zone of the concrete. Thus the lever arm is underestimated which is conservative.

Height of the compression zone:

$$x = \frac{Af_y}{0.8b_e f'_c} \leq h_s$$

The lever arm is:

$$z = m - 0.5x$$

So the moment of resistance M_u as described by equation (3.1) can be rearranged as follows:

$$M_u = 1.18M_{pl} + \Sigma S_u \left(z - \frac{1.18M_{pl}}{Af_y}\right) \tag{3.2}$$

This expression represents a linear relation between M and ΣS_u. The relation between the ultimate load and the degree of shear connection for the small-scale beams calculated with this simplified method is indicated by the dashed line in Fig. 16.

3.1.2 Beams with rigid non-ductile shear connectors

Fig. 17 shows the test results of small-scale beams with partial shear connection and rigid non-ductile shear connectors (block connectors), which are described in chapter 4, plotted against the theoretical relation between the ultimate load and the degree of shear connection determined with equation 3.1 (solid line) and equation 3.2 (dashed line). Apparently the experimental ultimate loads are smaller than the theoretical values. This is because the block-type shear connectors do not have sufficient deformation capacity to satisfy the assumptions of the plastic design methods for ductile connectors as described in 3.1.1.

Beams with partial shear connection and rigid non-ductile shear connectors can be designed according to a partial interaction theory, based on the real properties of the shear connection. This design method will be rather laborious and not suitable for practical use. Therefore it is better to base the design of such beams on the assumption that no slip occurs between the concrete slab and the steel beam. This is a safe assumption. If the stress-strain diagrams for steel and concrete are known, the relation between the ultimate moment M and the number of shear connectors for complete interaction can be calculated by the elasto-plastic method as is qualitatively shown in Fig. 18 (see also Fig. 6). In these calculations, in principle stresses due to pre-loading of the steel beam and due to shrinkage and creep of the concrete have to be taken into account. The calcu-

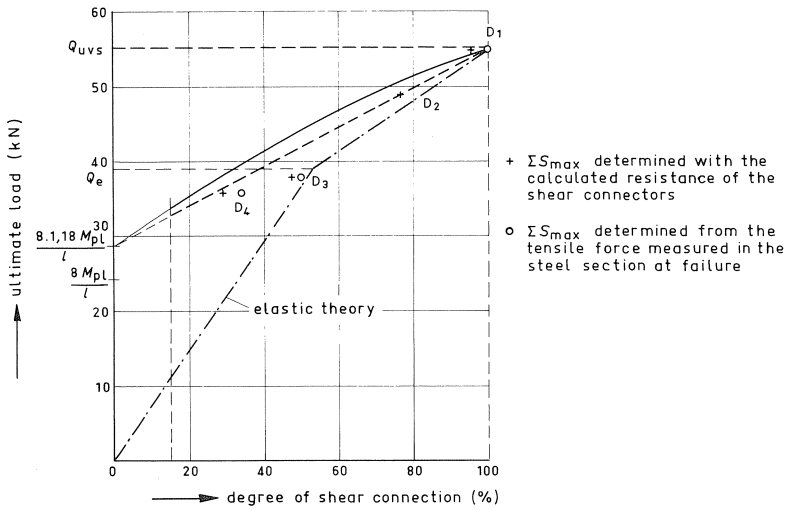

Fig. 17. Relation between the ultimate load and the percentage of rigid non-ductile shear connectors for simply supported beams with a uniformly distributed load.

lation of the elasto-plastic branch of the diagram is rather laborious. To simplify this calculation the curved part of the diagram can safely be approximated by a straight line. For this line the following equation can be derived:

$$N_{au} = \Sigma S_u = N_e + \frac{M_u - M_e}{M_{fsu} - M_e}(N_{fsu} - N_e) \tag{3.3}$$

For the small-scale beams this relation is also shown in Fig. 17. The figure shows that this method leads to safe values of the ultimate load as compared to the tests.

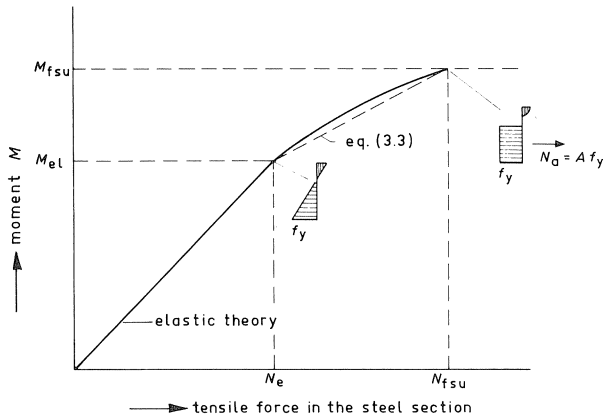

Fig. 18. Qualitative relation between the moment and the tensile force in the steel section with complete interaction (absolutely rigid).

3.2 *Ultimate load of continuous beams*

3.2.1 Introduction to the subject

The advantages of application of partial shear connection are so interesting that design methods have also been developed for continuous beams. These are discussed in this chapter. As an introduction the behaviour is illustrated with a theoretical model based on ideal plastic material behaviour. This model is definitely not presented as an operational model for the daily engineering practice. For that purpose the procedure is too laborious and, moreover, the basic assumptions are not necessarily sufficiently representative. The model is intended to qualitatively describe the influence of the resistance of the shear connection on the distribution of internal forces in a continuous beam. The charm of the model is that it provides more insight into the essential structural behaviour. The theoretical model is also important to explain the results of the tests described in chapter 4.
For use in design, two operational models, which are discussed in 3.2.3, have been derived from the theoretical model. As a consequence of the basic assumptions of the theoretical model, application of these operational practical methods has to be restricted to beams of which all parts satisfactorily approach ideal plastic material behaviour. Ideal plastic material behaviour may be assumed when the shear connectors are ductile and when the requirements for the application of the plastic theory or the elasto-plastic theory are met.
A calculation method for beams with rigid non-ductile shear connectors, which meet with the requirements for application of the plastic theory or the elasto-plastic theory, is given in 3.2.4.

3.2.2 A theoretical model based on ideal-plastic material behaviour

The theoretical model is applied to a beam over three supports and two equally long spans, as shown in Fig. 19. The load consists of a uniformly distributed load, simulated by 4 concentrated loads per span, similar to the test-set up for the small-scale beams described in chapter 4.
In Fig. 19 the longitudinal shear forces S_0 and S_i between the concrete slab and the steel beam are indicated by arrows. S_0 being the longitudinal shear force between the maximum sagging moment and the end support (external shear span), and S_i being the longitudinal shear force between the maximum sagging moment and the central support (internal shear span). The resistances of the shear connection are denoted by S_{ou} and S_{iu} for the external and the internal span respectively.
The ultimate load is dependant on the moments of resistance in the sagging and in the hogging moment sections. The relation is given by equation (3.4)

$$F_u = \frac{8M_{fu} + 3M_{su}}{l} \tag{3.4}$$

In this chapter a theoretical model is presented, which allows the determination of the

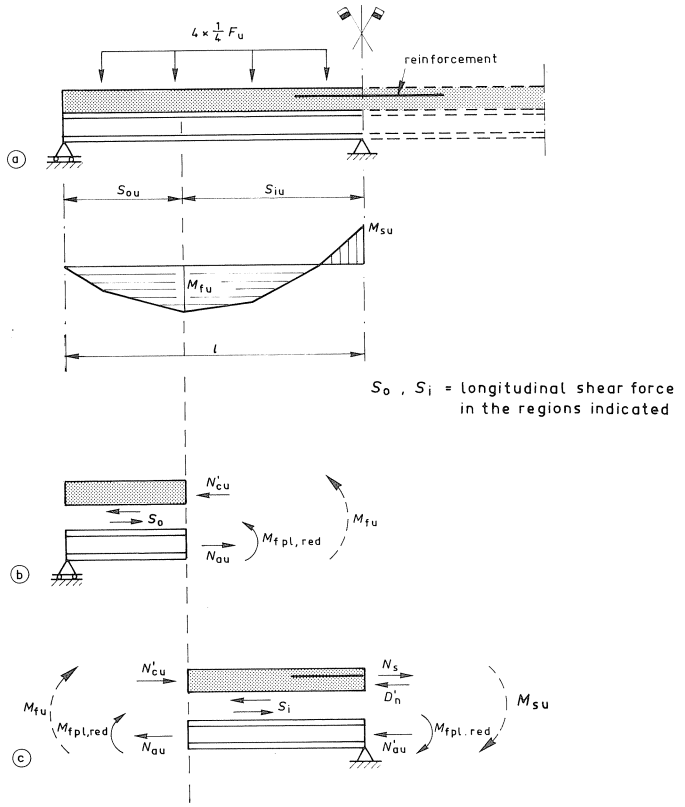

Fig. 19. Example.

influence of the resistances of the shear connection S_{ou} and S_{iu} on the ultimate load. The theoretical model is based on the following assumptions.

- The materials
  The reinforcement, the structural steel and the concrete are assumed to behave as ideal plastic materials. This means that the strain-stress relations can be schematically represented as shown in Fig. 20a.
- The shear connectors
  The shear connectors are assumed to be ideal ductile. As discussed before, this means that the relation between the shear force S and the slip δ can be schematically represented as shown in Fig. 20b.
- Further assumptions
  - tension stresses in the concrete are neglected;
  - plane cross-sections of the concrete slab and the steel section remain plane after bending;
  - the influence of the vertical shear force on the moment of resistance is neglected;
  - the width/thickness ratios of the parts of the steel beam are such that the effect of local buckling need not be taken into consideration (class 1 sections).

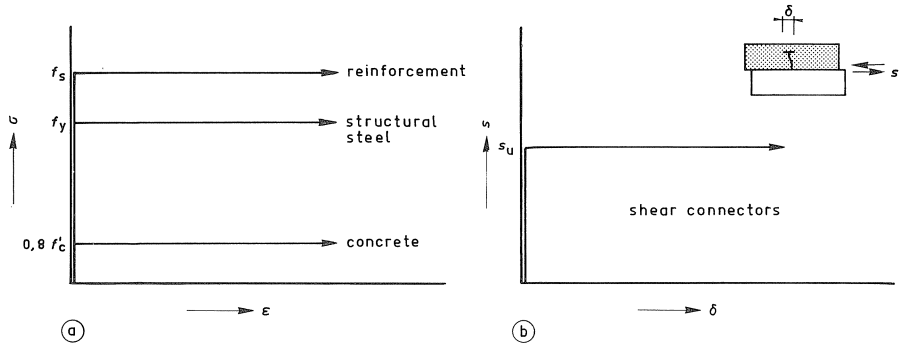

Fig. 20. Deformation characteristics of the materials and the shear connectors as assumed in the theoretical model.

3.2.2.1 Introduction to the presentation of the theoretical model

The simply supported beam, as already discussed in 3.1, is illustrative for the positive moment region of a continuous beam.
The moment M_{fu}, which is based on the stress distribution illustrated in Fig. 15, can be calculated with equation (3.6). The relation between M_{fu} and N'_{cu} is graphically represented in Fig. 21 (compare Fig. 6). To gain more insight, the contribution of each of the components as a function of the resistance of the shear connection has been qualitatively indicated. When $N'_{cu} = 0$, i.e. no shear connectors, then $M_{fu} = M_{pl}$ = plastic moment of the steel section. When $N'_{cu} = N_{au} = Af_y$ the moment is solely supplied by the normal forces N_{au} and N'_{cu} with the internal lever z. In [5] the minimum number of shear connectors is limited (50%), so that only a part of the curve is significant.

$$M_{fu} = N'_{cu} z + M_{pl,red} \tag{3.6}$$

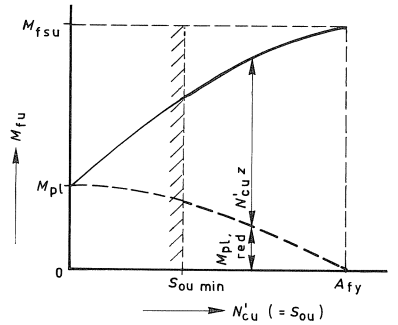

Fig. 21. Qualitative relation between N'_{cu} and M_{fu}.

A cantilever is illustrative for the negative moment region of a continuous beam and will be discussed hereafter.
Fig. 22 shows the example to be discussed with the internal forces acting on the con-

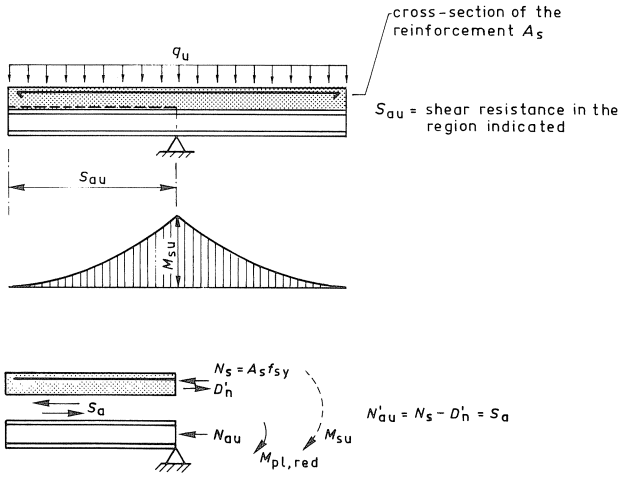

Fig. 22. Internal forces in a cantilever.

crete slab and the steel beam respectively (compare Fig. 19). At failure the reinforcement will allways yield so that $N_s = A_s f_{sy}$.

In the extreme case that no shear connectors are applied ($S_{au} = 0$) the equilibrium condition requires that the normal force in the concrete slab in the cross-section at the support has to be equal to zero. The tensile force in the reinforcement N_s has to be compensated by a compressive force D'_n, which develops at the underside of the cross-section of the concrete slab. The normal force N'_{au} in the steel beam is equal to zero. So at failure the unreduced plastic moment M_{pl} is present in the steel beam. The moment of resistance M_{su} is the sum of the moments in the reinforced concrete slab and the steel beam (see equation 3.7). Fig. 23a shows the distribution of the strains and the stresses.

$$M_{su} = N_s y_0 + M_{pl} \tag{3.7}$$

Another extreme case occurs when so many shear connectors are applied that $S_{au} \geq N_s$. Then the shear connection is defined as full shear connection. If tension stresses in the concrete are neglected $D'_n \geq 0$. From the equilibrium condition for the concrete slab follows that $D'_n = 0$ (because $D'_n = N_s - S_{au}$). The compressive force N'_{au} in the steel section is equal to N_s. The corresponding stress distribution has already been discussed in chapter 2 (see Fig. 14), and has also been included in Fig. 23 for comparison. It has been assumed that $N_s < Af_y$, which will always occur in practical cases. So the moment M_{su} can be calculated with the following equation:

$$M_{su} = N_s y + M_{pl,red} = M_{fsu} \tag{3.8}$$

If partial shear connection is applied and so $S_{au} < N_s$, it follows from the horizontal equilibrium of the concrete slab and the steel section that:

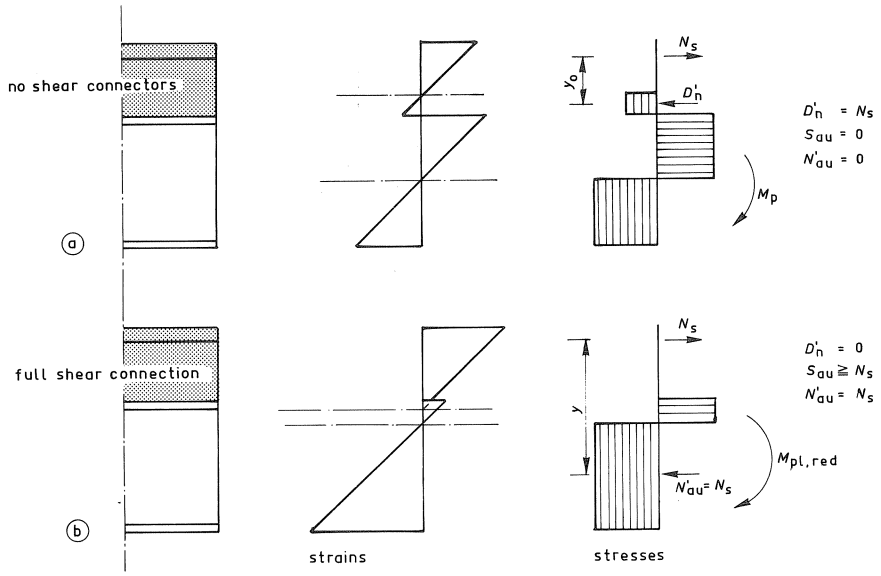

Fig. 23. Distributions of strains and stresses for two extreme values of S_{au}.

$$N'_{au} = S_{au} \tag{3.9}$$

$$D'_n = N_s - S_{au} \tag{3.10}$$

The normal forces in the concrete slab and the steel section are known. The moment of resistance M_{su} can be derived from the optimum stress distribution corresponding to these normal forces, as is shown in Fig. 24. The figure also shows how this stress distribution can be split up into 3 components, from which the corresponding moment can easily be calculated with the following equation:

$$M_{su} = N'_{au}\, y + D'_n\, y_0 + M_{pl,red} \tag{3.11}$$

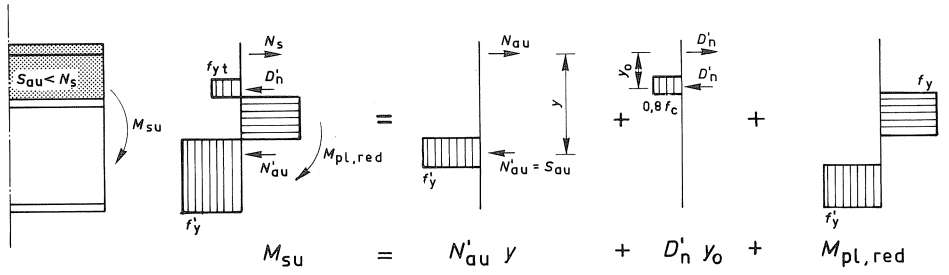

Fig. 24. Stress distribution in case of a partial shear connection.

The relation between M_{su} and S_{au} is determined by the equations (3.9), (3.10) and (3.11). Fig. 25 qualitatively shows this relation. When the parameter on the horizontal axis is changed, this diagram also shows the relation between M_{su} and D'_n. This relation will

prove to be of importance in the discussion of continuous beams. It is useful to draw the negative axis for the hogging moments M_{su} upwards along the vertical axis. To gain better insight, Fig. 26 qualitatively shows the contribution of the three components of equation (3.11) as functions of the resistance of the shear connection.

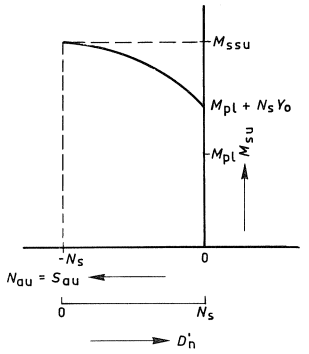

Fig. 25. The relation between M_{su} and S_{au} and M_{su} and D'_n.

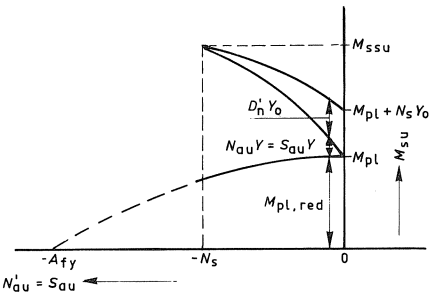

Fig. 26. Components of M_{su}, when dependent on the shear capacity S_{au}.

Fig. 19 shows the continuous beam schematically cut at the support and at the maximum sagging moment. It would seem obvious to also cut the beam at the points of contraflexure, which would reduce the theoretical model to the simply supported case and the cantilever already discussed. However, it will be proved hereafter, that although the resulting moment in the point of contraflexure is zero, the normal forces and the moments in the steel beam and the concrete slab do not necessarily have to be zero too. As illustrated in Fig. 13, the optimum stress distributions corresponding to M_{fsu} and M_{ssu} only occur when the resistance of the shear connection meets both of the following requirements. When at least one of these requirements is not met, the shear connection is defined as partial shear connection.

$$S_{ou} \geq Af_y$$

$$S_{iu} \geq Af_y + A_s f_{sy}$$

The theoretical model discussed hereafter elaborates on the distribution of the internal forces in the composite beam and makes it possible to determine the relation between the ultimate load and the resistances of S_{ou} and S_{iu} within the scope of the assumptions described before. The concrete slab and the steel beam of each part of the shear span shown in the Figs. 19b and c, with the relevant normal and shear forces, will be discussed separately.

3.2.2.2 The external shear span (Fig. 19b)

This part is similar to the part of the simply supported beam already discussed. The relation between M_{su} and N'_{cu} according to equation (3.6) is qualitatively shown in Fig. 21. As will become clear below, in a continuous beam it may not simply be assumed that N'_{cu} is equal to S_{ou} when $S_{ou} \leq Af_y$. This is an important difference between simply supported and continuous beams.

3.2.2.3 The internal shear span (Fig. 19c)

From the condition of horizontal equilibrium of the concrete slab follows:

$$N'_{cu} + N_s - S_i - D'_n = 0 \tag{3.12}$$

From the condition of horizontal equilibrium of the cross-section at the support follows:

$$N'_{au} - N_s + D'_n = 0 \tag{3.13}$$

For comparison with the equations (3.9) and (3.10) the following expressions for N'_{au} and D'_n can be derived:

$$N'_{au} = S_i - N'_{cu} \tag{3.14}$$

$$D'_n = N_s - S_i + N'_{cu} \tag{3.15}$$

If (3.15) is compared with (3.10) it will become evident that, contrary to the cantilever, in this beam the compressive force D'_n may be larger than N_s. In that case apart from the tensile force in the reinforcement, also a part of N'_{cu} is compensated by the compressive force D'_n. This proves that the normal forces and therefore also the moments in the steel beam and the concrete slab are not necessarily equal to zero at the points of contra-flexure. It is relevant for the rest of the discussion to know which limits are valid for the values of N'_{au} and D'_n assuming N_s to be smaller than Af_y.
As tension stresses in the concrete are neglected $D'_n \geq 0$ is valid. Then equation (3.13) leads to $N'_{au} \leq N_s$. The normal force N_{au} is a compressive force when $D'_n < N_s$, equal to zero when $D'_n = N_s$ and a tensile force when $D'_n > N_s$.
The theoretical maximum value of D'_n is reached when the force in the steel beam N_{au} is equal to a tensile force Af_y. The value of D'_n is also limited by the condition that, assuming ideal plastic material behaviour, the height of the compression zone can only

be equal to the distance between the bottom surface of the reinforcement and the bottom surface of the concrete slab.

$$D'_{n,max\,1} = Af_y + N_s$$

$$D'_{n,max\,2} = b_e h'_s 0.8 f'_c$$

Fig. 27 shows characteristic stress distributions in the cross-section at the internal support for some values of N'_{au} and D'_n.

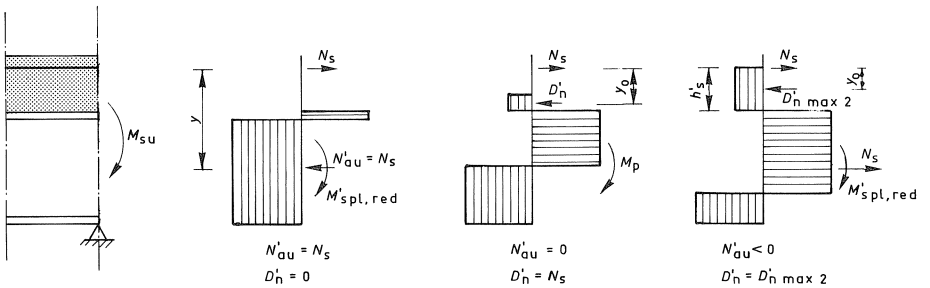

Fig. 27. Some characteristic stress distributions in the cross-section at the internal support.

With the equations (3.11) and (3.13) not only the relation between M_{su} and N'_{au} but also the relation between M_{su} and D'_n can be determined. Fig. 28 qualitatively shows these relations. For comparison with Fig. 26, Fig. 28 also shows the contribution of the three components to equation (3.11) when N_a is a tensile force $(D'_n > N_s)$.
Fig. 28 shows that it is physically possible for the value of M_{su} to become smaller than M_{pl}, and even that M_{su} becomes positive if N_{au} is a large tensile force. Of course the

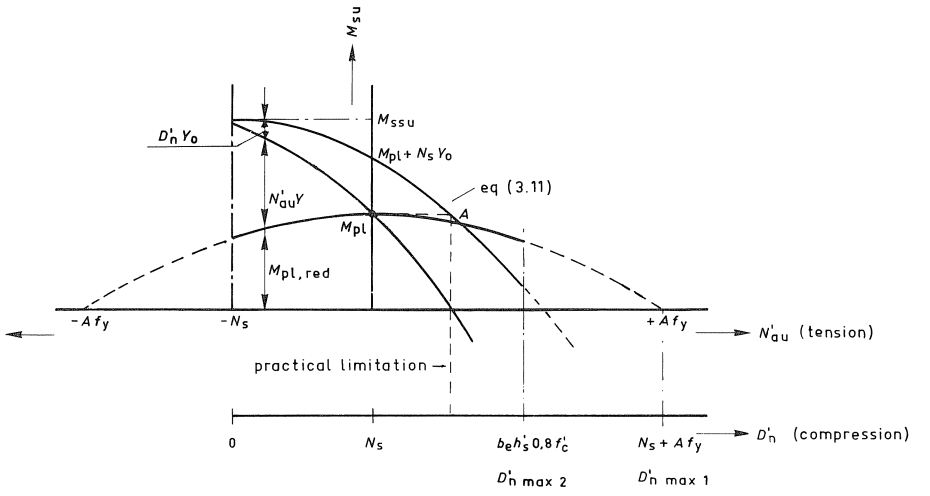

Fig. 28. Relation between M_{su} and N_{au} and M_{su} and D'_n in a continuous beam.

design is not very practical if M_{su} appears to be smaller than M_{pl} (point A in Fig. 28). This leads to a practical limitation for D'_n and N_{au}. Further practical limitations of D'_n and N_{au} may result from the following aspects:
- the shear connectors do not allow the necessary slip;
- the strain ε'_c of the concrete is limited (for example 3.5‰).

3.2.2.4 Calculation of the ultimate load

The calculation of the example shown in Fig. 19 would be simple when the relation between the resistances S_{ou} and S_{iu} were known, which would result in shear failure of the shear connectors in both parts of the beam. In that case, $S_0 = S_{ou}$ and $S_i = S_{iu}$. The values of N'_{cu} and D'_n could then be calculated with equations (3.5) and (3.15):

$$N'_{cu} = S_0 = S_{ou}$$

$$D'_n = N_s - S_{iu} + S_{ou}$$

Subsequently, the values of M_{fu} and M_{su} could be determined with the relations according to the Figs. 21 and 28 and the ultimate load F_u would follow simply from equation (3.4). Unfortunately the required relation of S_{ou} and S_{iu} is not known, which means that with a random chosen value of S_{ou} and S_{iu} it is not definitely certain that both longitudinal shear planes are critical.
For this reason only S_{iu} is chosen in the theoretical model discussed below, so that $S_i = S_{iu}$. With a chosen value for S_{iu} and a known value for N_s the horizontal equilibrium condition can still be satisfied with infinite combinations. Now applies:

$$N'_{cu} + N_s - S_{iu} - D'_n = 0 \qquad \text{(see also 3.12)} \tag{3.16}$$

If in addition to the choice of S_{iu}, also a value for D'_n is chosen, equation (3.16) directly leads to a value for N'_{cu}. The value of $S_{ou}(= N'_{cu})$ follows from the equilibrium condition for the external shear span. Now that the values of N'_{cu} and D'_n are known, consequently M_{fu} and M_{su}, and F_u will result from equation (3.4).
Subsequently, with a fixed value of S_{iu}, this can be repeated for different values of D'_n. Now, in accordance with Prager's laws, a value of D'_n will occur that leads to the largest ultimate load. This value is indicated by $\bar{D}'_n$. The corresponding values of N'_{cu} and S_{ou} are indicated by $\bar{N}'_{cu}$ and $\bar{S}_{ou}$. Application of more shear connectors than required for $\bar{S}_{ou}$, in the external shear span, does not lead to a higher ultimate load than with $\bar{S}_{ou}$. If S_{ou} is chosen smaller than $\bar{S}_{ou}$, then for $D'_n = \bar{D}'_n - (\bar{S}_{ou} - S_{ou})$ the ultimate load is as large as possible with the chosen distribution of shear connectors.
From this description it follows that the determination of D'_n is critical for the solution of the problem. This reflects the essence of the theoretical model. The procedure is schematically shown in the flow diagram in Fig. 29.
Fig. 30 shows a graphical illustration of the optimization procedure. With equation (3.16), in which $(S_{iu} - N_s)$ is known, the relation between M_{fu} and N'_{cu} can be transformed into a relation between M_{fu} and D'_n, and can subsequently be combined with the relation between M_{su} and D'_n. Then, using equation (3.4) the relation between F_u and D'_n

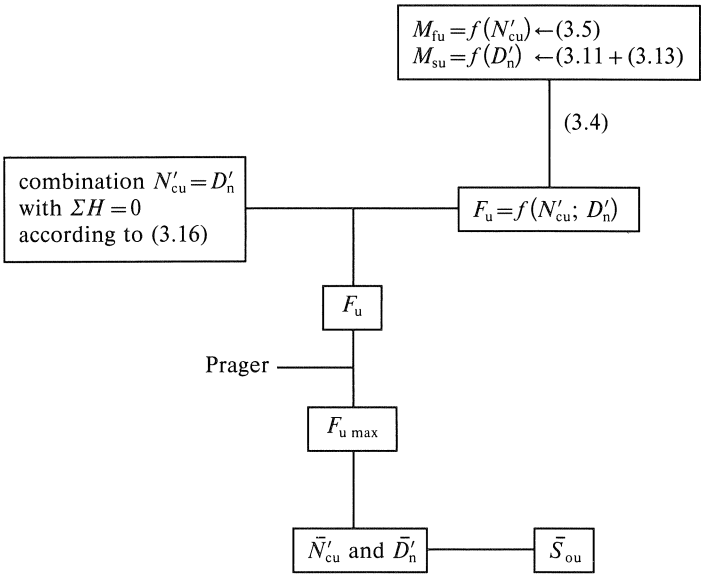

Fig. 29. Flow diagram of the optimization procedure

can be derived. The real ultimate load will be the maximum value of F_u and is indicated by $\bar{F}_u$. Then, with the corresponding value of the compressive force $D'_n(=\bar{D}'_n)$ from equation (3.15), the corresponding value of $N'_{cu}(=\bar{N}'_{cu})$ can be determined. From the condition $\bar{S}_{ou}=\bar{N}'_{cu}$ now follows the minimum required shear resistance $\bar{S}_{ou}$ in the external shear span.
With this optimization procedure it is possible to derive equations to determine $\bar{F}_u$, $\bar{D}'_n$ and $\bar{S}_{ou}$.

3.2.2.5 Influence of the longitudinal shear resistance

The influence of S_{ou}
From the optimization procedure discussed before followed that for each value of S_{iu} and N_s a value of $S_{ou}=\bar{S}_{ou}$ exists which leads to a maximum for the ultimate load $(\bar{F}_u)$. The corresponding distribution of the shear connectors is referred to as "a harmonised distribution of shear connectors". When S_{ou} is chosen larger than $\bar{S}_{ou}$ the ultimate load will not become larger than $\bar{F}_u$. When the shear resistance in the external shear span is chosen smaller than $\bar{S}_{ou}$, for example $0.6\bar{S}_{ou}$, N'_{cu} cannot reach the optimum value $\bar{N}'_{cu}$, and cannot exceed $0.6\bar{S}_{ou}$.
In this case D'_n follows directly from the horizontal equilibrium condition of the concrete slab in the internal shear span, namely:

$$D'_n=0.6\bar{S}_{ou}+(N_s-S_{iu})$$

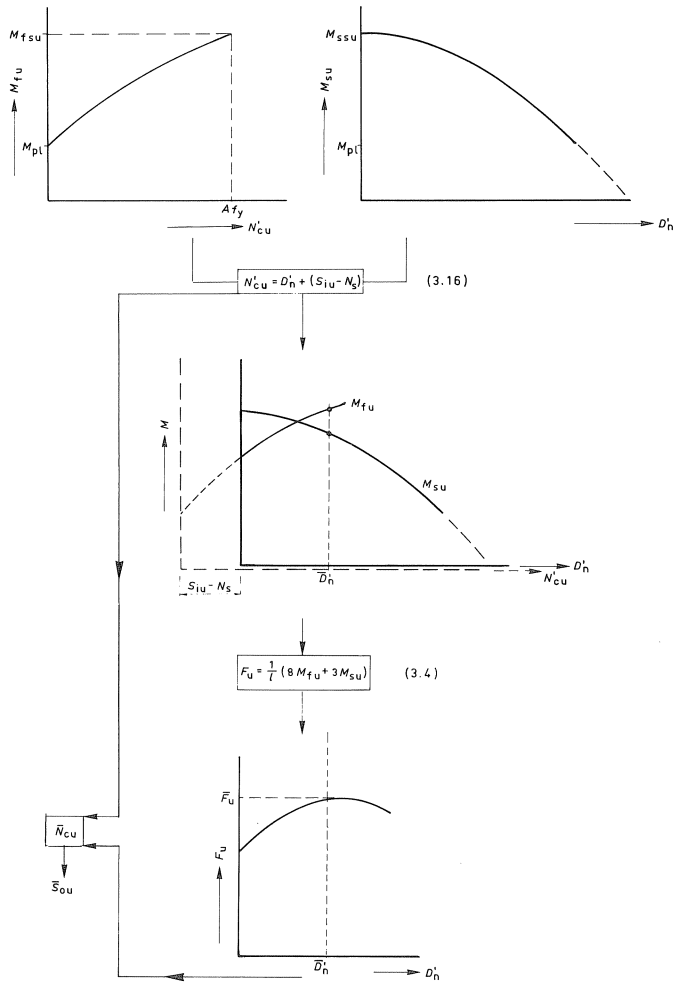

Fig. 30. Graphical representation of the optimization procedure.

The graphical representation in Fig. 31 clearly shows that a smaller value of S_{ou} compared to $\bar{S}_{ou}$ (for example $S_{ou} = 0.6\bar{S}_{ou}$) results in a value of the ultimate load smaller than $\bar{F}_u$.

The influence of S_{iu}

In the discussion of the theoretical model up till now a given value of S_{iu} was assumed, leading to F_u and $\bar{F}_u$. Variation of S_{iu} makes it possible to determine the relation between F_u and S_{iu} and also between S_{ou} and S_{iu}. Fig. 32 qualitatively shows these relations for $S_{ou} = \bar{S}_{ou}$ ("harmonised distribution") and for $S_{ou} = 0.6\bar{S}_{ou}$ ("not-harmonised distribution").

For the combinations of S_{ou} and S_{iu} in the shaded area of Fig. 32b applies that $N'_{cu} < S_{ou}$, even when $S_{ou} < Af_y$. Fig. 32 shows how the required values of S_{ou} and S_{iu} can be estab-

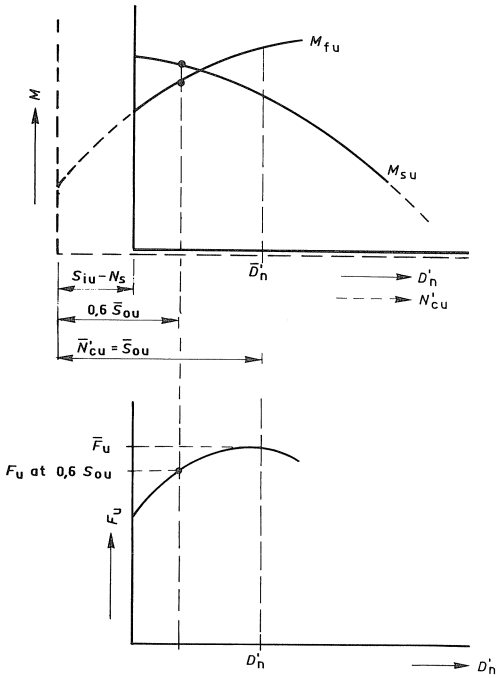

Fig. 31. Graphical representation of the calculation procedure when $S_{ou}=0.6\bar{S}_{ou}$.

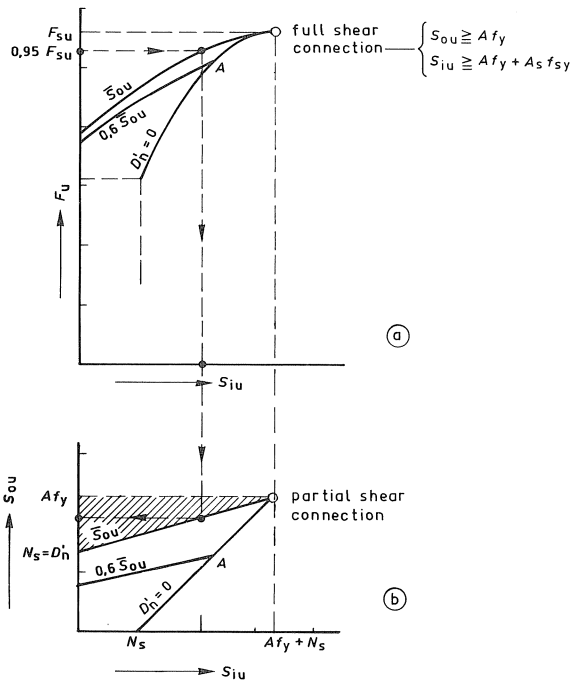

Fig. 32. Relation between F_u and S_{iu} and between S_{ou} and S_{iu}.

lished for an arbitrary value of F_u, for example $0.95F_{su}$. In this example S_{ou} is assumed to be harmonised with S_{iu}.
The minimum value of D'_n is equal to zero. The point on the $0.6\bar{S}_{ou}$ curves in Fig. 32, where this is the case, is indicated by the letter A. The position of these points A in the diagram for different values of $S_{ou}/\bar{S}_{ou}$ can easily be derived.
When $D'_n = 0$ the value of N'_{cu} follows directly from the horizontal equilibrium condition of the concrete slab in the internal shear span. M_{fu} is then also known and subsequently F_u corresponding to point A can be calculated. $N'_{cu} = S_{ou}$ leads to the value of S_{ou} corresponding to point A.

The influence of the total number of shear connectors $(S_{ou} + S_{iu})$
As appears from Fig. 32, an arbitrary value for S_{iu} will result in the largest value of the ultimate load when S_{ou} is harmonised with $S_{iu}(S_{ou} = \bar{S}_{ou})$. This does not imply that when $S_{ou} = \bar{S}_{ou}$ the total number of shear connectors for a given value of F_u is minimal. This is because $S_{ou} + S_{iu}$ is relevant for the total number of shear connectors required. To illustrate this, Fig. 33 shows the relation between the ultimate load F_u and the total shear resistance $S_{ou} + S_{iu}$ (in non-dimensional format). Contrary to Fig. 31 the lines of $S_{ou} < \bar{S}_{ou}$ now intersect the line of $S_{ou} = \bar{S}_{ou}$.

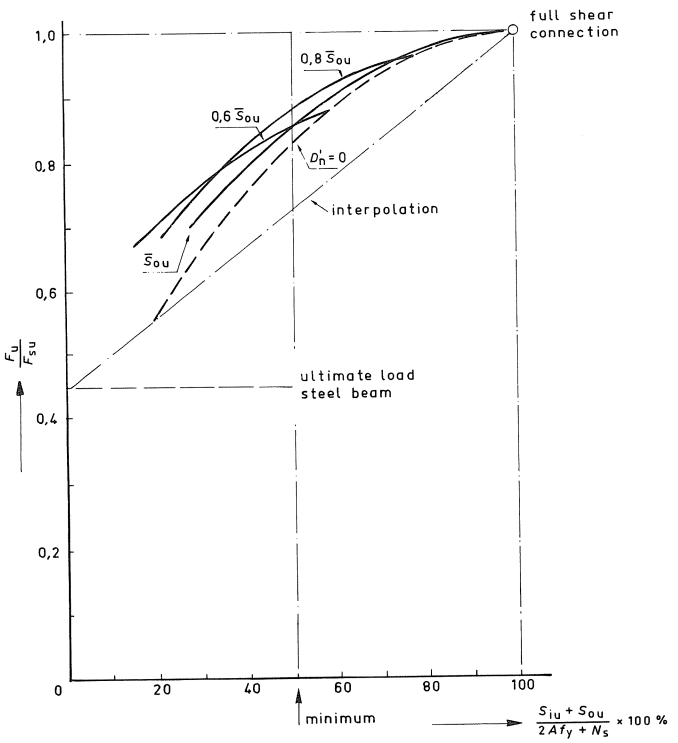

Fig. 33. Qualitative relation between the calculated ultimate load and the degree of shear connection for some distributions of shear connectors.

In the assessment of Fig. 33 it has to be kept in mind that in design standards the minimum number of shear connectors is limited. In the 1985 Draft of Eurocode 4 this limit is 50%. If the degree of shear connection is over 50% the differences in the values of the ultimate loads for the various distributions of the ductile shear connectors are relatively small.
The figure also includes the relation between F_u and $S_{ou} + S_{iu}$, which is obtained when the increase of the strength caused by composite action, is assumed to be directly proportional to the degree of shear connection applied. This relation will be applied in one of the simplified methods discussed below.

3.2.3 Design rules for beams with ductile shear connectors

3.2.3.1 Direct choice of D'_n

As has already been stated in 3.2.1 the theoretical model discussed there is too laborious for the daily engineering practice. This is mainly caused by the necessary optimization procedure of D'_n to $\bar{D}'_n$. The simplified method discussed here is based on the choice of a value for D'_n, without further optimization. As appears from Fig. 30, an arbitrary choice for D'_n will always lead to a safe value of the ultimate load F_u. An obvious choice is $D'_n = 0$. From equation (3.13) follows that this also implies $N'_{au} = N_s$.
With fixed values of S_{iu} and N_s, N'_{cu} follows directly from the horizontal equilibrium condition for the concrete slab in the internal shear span. When N'_{cu} and $D'_n(=0)$ are known, M_{fu} and M_{su} are determined with the equations (3.6) and (3.11). Then the value of F_u can be determined (see Fig. 19).
The value of S_{ou} follows from $N'_{cu} = S_{ou}$. The relation between F_u and $S_{ou} + S_{iu}$ can be found by doing this calculation several times for various values of S_{iu}. The results of the tests on small-scale beams described in chapter 4, are indicated by a dashed line in Fig. 33. For comparison with the Figs. 30 and 31, Fig. 34 shows a graphical representation of the calculation procedure.
It has to be noted that a 10% reduction of the maximum ultimate load leads to a reduction of about 40% in the required shear resistance. In comparison to this reduction the "profit", which can be obtained by optimizing D'_n is negligible. Fig. 33 also shows that, in

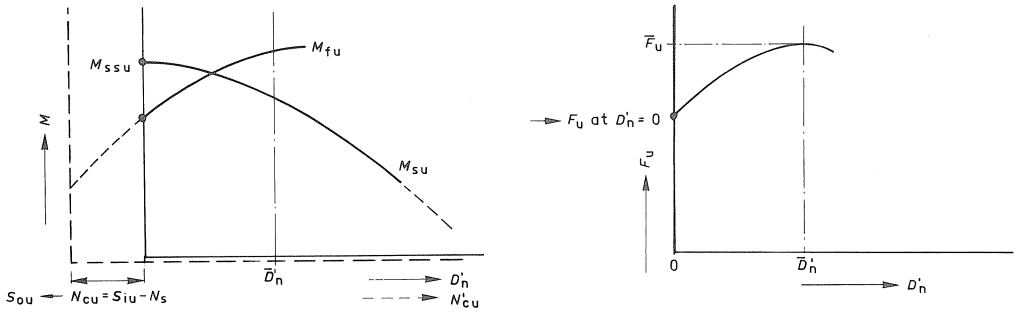

Fig. 34. Graphical representation of the calculation procedure when $D'_n = 0$.

this example, the saving resulting from the more complicated method only becomes relevant when the degree of shear connection is smaller than 50%.
The previous discussion was based on an assumed value of S_{iu}, and subsequent calculation of F_u and S_{ou}. The relation between F_u and $S_{uo} + S_{ui}$ could be established by varying S_{iu}. However, in a design calculation the dimensions of the beam and the reinforcement over the supports (N_s) are usually chosen and the required F_u is known. In that case the beam over three supports shown in Fig. 19, is calculated as follows.
Equation (3.4) results in:

$$F_u = \frac{8M_{fu} + 3M_{su}}{l}$$

From the assumption $D'_n = 0$ follows:

$$N'_{au} = N_s$$

$$M_{su} = N_s y + M_{pl,red} = M_{ssu} \qquad \text{(see Fig. 15)}$$

When F_u is known and M_{su} has been determined, the required value of M_{fu} can be calculated. Equation (3.6) then leads to N'_{cu} (see Fig. 21) and subsequently the required shear resistance S_{ou} follows from:

$$S_{ou} = N'_{cu}$$

The required shear resistance of the internal span then results from:

$$S_{iu} = S_{ou} + N_s$$

3.2.3.2 The interpolation method

This simplified method is based on the determination of the ultimate load of a beam with partial shear connection by linear interpolation between the ultimate load of the steel beam and the ultimate load of the composite beam with full shear connection, dependent on the degree of shear connection. The corresponding relation between F_u and $S_{ou} + S_{iu}$ has already been qualitatively shown in Fig. 33. For the sake of clarity this relation is shown once more in Fig. 35 (compare Fig. 7).
Now the calculation is as follows. The ultimate load F_{su} for full shear connection and the corresponding number of shear connectors are calculated with the method described in chapter 2.2. For a beam over three supports this is illustrated in Fig. 13. Next the ultimate load F_{ou} of the steel beam without composite action is calculated with the plastic hinge theory.
For each value of F_u smaller than F_{su} the required degree of shear connection can be determined by linear interpolation (Fig. 33). Apart from the degree of shear connection also the distribution over the separate parts of the beam has to be known. For the beam over three supports as shown in Fig. 19, this means that apart from $S_{ou} + S_{iu}$ also S_{ou} and S_{iu} have to be determined separately. If the relation is assumed to be the same as for a full shear connection this will always result in safe values of the ultimate load. For the

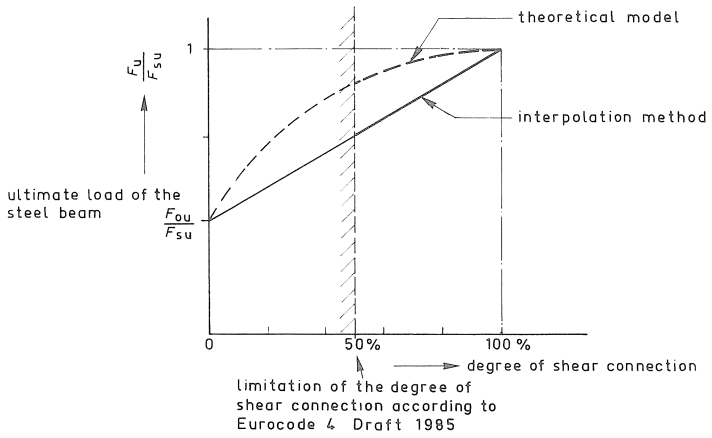

Fig. 35. Qualitative relation between the calculated ultimate load and the degree of shear connection with the interpolation method.

beam over three supports with equal spans (Fig. 19) this leads to:

$$n_i = \frac{S_{iu}}{S_{ou} + S_{iu}} = \frac{Af_y + N_s}{2Af_y + N_s} \qquad \text{(see Fig. 13)} \tag{3.17}$$

The interpolation method is easy to use and links up well with the methods for simply supported beams described elsewhere in this chapter.
It was described before how the number of shear connectors and the distribution over the beam can be determined when F_u is known. Vice versa, F_u can be calculated when the number of shear connectors and the distribution are known. This may not simply be based on the total number of shear connectors in a span, as it is not known whether S_{ou} is harmonised with S_{iu}. To be sure it is best to do the calculation for each of the parts of the beam separately. Then the calculation for the beam over three supports as shown in Fig. 19 is as follows:

$$\text{for the external shear span: } F_u = F_{ou} + \frac{S_{ou}}{Af_y}(F_{su} - F_{ou}) \tag{3.18}$$

$$\text{for the internal shear span: } F_u = F_{ou} + \frac{S_{iu}}{Af_y + A_s f_{sy}}(F_{su} - F_{ou}) \tag{3.19}$$

The smallest of the two values for F_u is critical.

3.2.4 Design rules for beams with non-ductile shear connectors

Since a more subtile method is not yet available, it has to be assumed for safety, that no slip occurs between the concrete slab and the steel beam when rigid non-ductile shear connectors are applied. The concrete slab and the steel beam are assumed to have the same neutral axis.

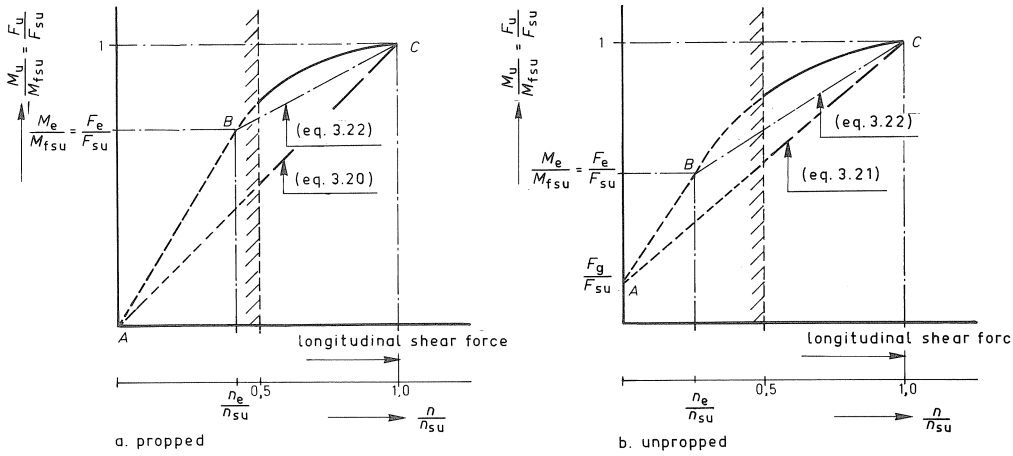

Fig. 36. Relation between the load and the overall shear force, i.e. the required degree of shear connection, with the simplification according to [7].

A relation between the load and the shear force (= the required degree of shear connection) is generally found as schematically shown in Fig. 36. (compare Figs. 7 and 18). This figure shows that a safe value of the required degree of shear connection is found with the following equation:

$$n = \frac{F_u}{F_{su}} n_{su} \tag{3.20}$$

When the beam is unpropped the following equation may also be used:

$$n = \left(\frac{F_u - F_g}{F_{su} - F_g} \right) n_{su} \tag{3.21}$$

In 3.1 a more optimal approach for simply supported beams was given. It was suggested to use a bi-linear relation consisting of the elastic branch to F_{el} and a linear approximation of the curved elasto-plastic branch. The relation according to this method is indicated by the dash-dot line in Fig. 36. The following equation belongs to the linear approach of the elasto-plastic branch BC (compare equation 3.3):

$$n = n_e + \left(\frac{M_u - M_e}{M_{fsu} - M_e} \right) (n_{fsu} - n_e) \tag{3.22}$$

4 Experimental verification

For the verification of the design methods described in the chapters 2 and 3, a series of tests on small-scale beams were carried out at TNO-IBBC. The test programme and the test results of the simply supported beams will be discussed in 4.1. The tests on continuous beams will be discussed in 4.2.

Also some tests on full-scale simply supported and continuous beams were carried out at TNO-IBBC. These tests confirm the results of the tests on the small-scale beams. A description can be found in [1] and [2].

4.1 *Tests on small-scale simply supported beams*

4.1.1 The test programme

A series of 14 small-scale beams were tested, the dimensions of which are given in Fig. 37. The test beams may be considered as small-scale models with a scale of about 1 : 3. All beams were subjected to an eight point load, as is schematically shown in Fig. 38. This is a simulation of equally distributed loading conditions.

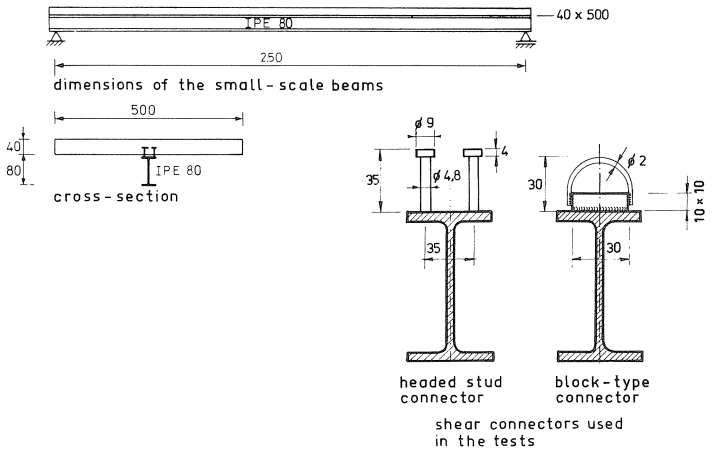

Fig. 37. Dimensions of the small-scale beams and the shear connectors used.

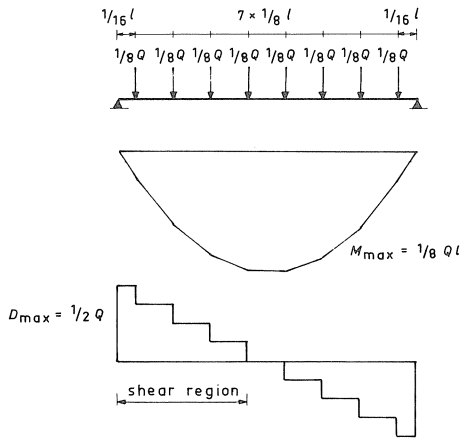

Fig. 38. Load arrangement.

Fig. 39 shows the test set-up. The influence of the following variables was examined:

a. The type of shear connector.
   - ductile shear connectors: headed studs ⌀ 4.8 (see Fig. 37);
   - rigid shear connectors: block ⏍ 10 (see Fig. 37).

b. The number of shear connectors.
   In Table 1 the degree of shear connection is given as $nS_{max}/N_{au} \times 100\%$. In all tests the shear connectors were uniformly distributed over the shear span (see Fig. 38).

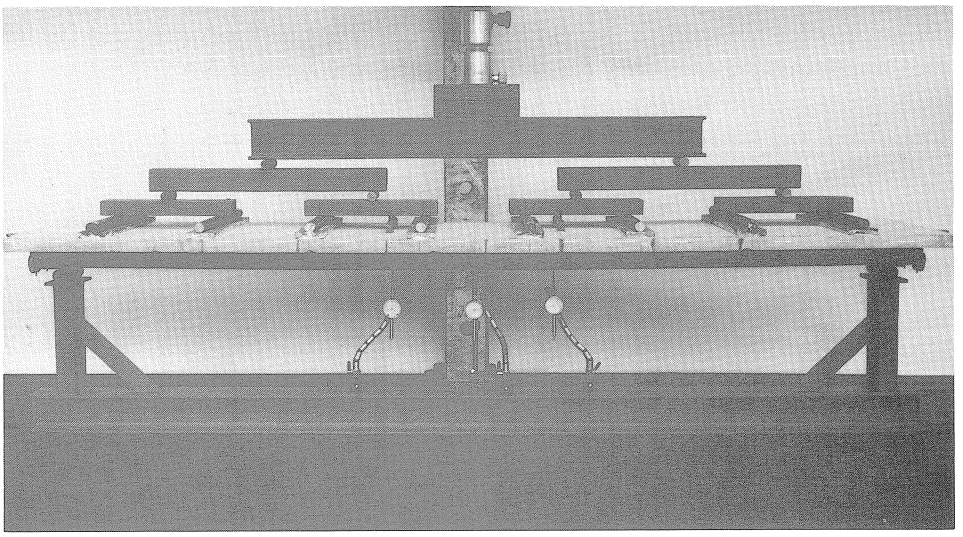

Fig. 39. The test set-up.

Table 1. Test programme

test beam	shear connector	degree of shear connection (%)	concrete grade	bond	pre-load
C1	headed stud	101	K 300	prevented	propped
C2		77	K 300	prevented	propped
C3		49	K 300	prevented	propped
C4		27,5	K 300	prevented	propped
C5		26,5	K 300	not prevented	propped
C6		100	K 300	prevented	unpropped
C7		50	K 300	prevented	unpropped
C8		26,5	K 300	prevented	unpropped
D1	block-type	96	K 300	prevented	propped
D2		77	K 300	prevented	propped
D3		48	K 300	prevented	propped
D4		29	K 300	prevented	propped
D5		102	K 450	prevented	propped
D6		30	K 450	prevented	propped

c. The natural bond of the concrete slab to the steel beam.
The natural bond was prevented by applying a debonding agent, except in test beam C5.
d. The concrete grade.
e. Propped or unpropped construction.
The pre-loading of the unpropped beams was imitated by imposing a deflection on the steel beam before the casting of the concrete, to such an extent that the maximum bending stress had the following value:

$$\sigma_{max} = \frac{Z_{pl} f_y}{Z_{el} \gamma} = 1.15 \frac{240}{1.4} \approx 200 \text{ N/mm}^2$$

4.1.2 Material properties

The relevant properties of the materials used for the small-scale beams are summarized in Table 2.

Table 2. Material properties

	concrete slab		steel beam			shear connectors		
test beam	f'_{ck} (N/mm^2)	E'_c (kN/mm^2)	A (mm^2)	Z_{pl} (mm^3)	f_y (N/mm^2)	n	S_{max} (kN)	$\frac{nS_{max}}{Af_y}$ 100 (%)
C1	30	33	812	24600	292	33	7,25	101
C2	30	33	812	24600	292	25	7,25	77
C3	30	33	812	24600	292	16	7,25	49
C4	30	33	812	24600	292	9	7,25	27,5
C5	30	33	822	25000	300	9	7,25	26,5
C6	30	33	822	25000	300	34	7,25	100
C7	30	33	822	25000	300	17	7,25	50
C8	30	33	822	25000	300	9	7,25	26,5
D1	32	34	804	24400	310	10	24	96
D2	32	34	804	24400	310	8	24	77
D3	32	34	804	24400	310	5	24	48
D4	32	34	804	24400	310	3	24	29
D5	48	38	806	24400	302	10	25	102
D6	46	37	806	24400	302	3	25	30

For the concrete so-called micro-concrete was used, the composition of which was based on a scale factor of 1 : 3. The strength of the concrete was determined on test cubes of 70 × 70 × 70 mm, on the same day that the beams were tested.
The strength of the shear connectors was determined with small-scale push-out tests.

4.1.3 Test results and conclusions

Table 3 shows a comparison between the calculated values of the moments of resistance (calculated with the methods given in 2.1 and 3.1) and the maximum moments resulting from the tests. With the exception of tests D4 and D6, the theoretical values correspond reasonably well with the test values. The calculated values are all conservative. For the tests D4 and D6 the difference is rather large. This will be discussed later.

Table 3. Test results

test beam	shear connector	degree of shear connection (%)	$M_{u,theory}$ (kNm)	$M_{u,test}$ (kNm)	$\frac{M_{u,test}}{M_{u,theory}} 100$ (%)
C1	headed stud	101	15,4	17,3	112
C2		77	15,1	15,4	102
C3		49	13,0	13,6	104
C4		27,5	11,2	11,5	103
C5		26,5	11,5	12,4	108
C6		100	17,0	17,4	102
C7		50	13,6	15,6	114
C8		26,5	11,5	12,6	110
D1	block-type	96	16,8	17,0	101
D2		77	14,8	15,2	103
D3		48	11,0	11,8	107
D4		29	6,6	11,2	170
D5		102	17,8	17,9	100
D6		30	7,2	11,0	152

In Fig. 40 the measured load-deflection curves for the beams C1 to C4 inclusive are given. This figure shows clearly that, with partial shear connection, the ultimate load is indeed dependent on the degree of shear connection. But it also shows clearly that the ultimate load of a beam with only a 25% shear connection is more than 66% of the ultimate load of a beam with full shear connection.
In Fig. 41 the measured load-deflection curves for the beams with block-type connectors are given. A comparison with Fig. 40 shows that these beams with partial shear connection failed rather suddenly (small deformation capacity). To illustrate the influence of slip, as discussed in chapter 1, Fig. 42 shows the load-deflection curves for the beams C4 (bond prevented) and C5 (with natural bond).

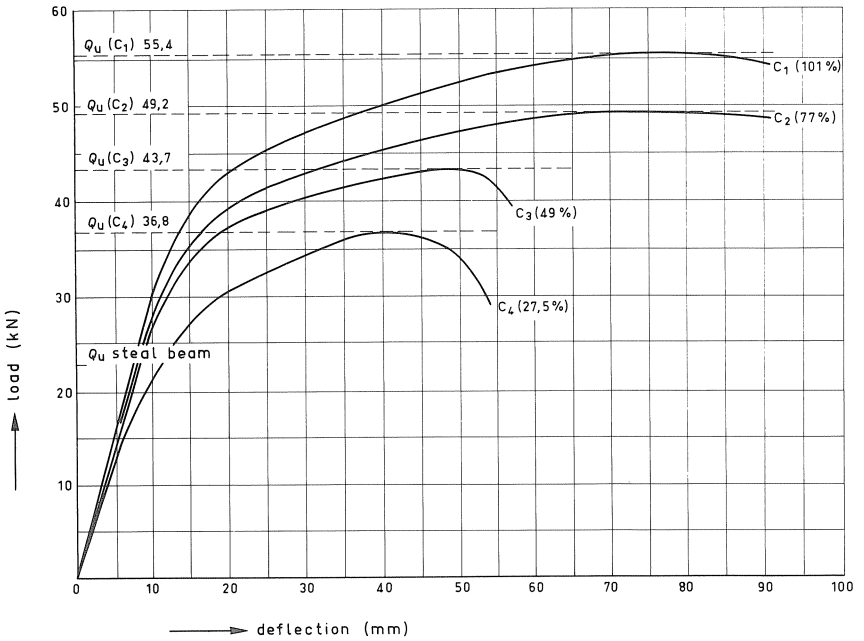

Fig. 40. Load-deflection curves for the test beams with headed stud connectors.

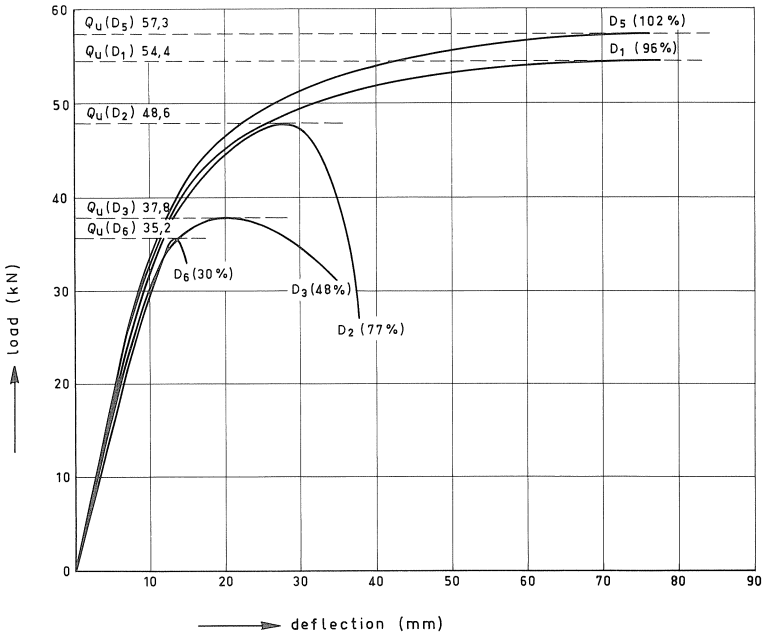

Fig. 41. Load-deflection curves for the test beam with block-type shear connectors.

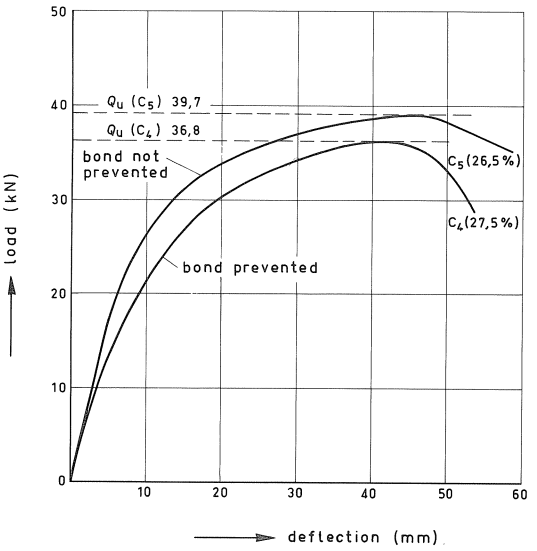

Fig. 42. Load-deflection curves for test beams C4 and C5.

Fig. 43 shows the measured M-$\varkappa$ curves of the beams C6 to C8 inclusive. The Figs. 44 to 46 inclusive show the M-$\varkappa$ curves of comparable beams, which were either propped or unpropped.

Comparison of these curves shows that for propped beams the moment M_{el} decreases when a lower degree of shear connection is used. In the unpropped beams the moment M_{el} is practically independent of the degree of shear connection. This is caused by the fact that the tensile force in the steel beam at moment M_{el} is smaller in unpropped beams due to the more favourable stress distribution in the steel beam. This also means that the force on the shear connectors, and therefore the slip, is smaller.

Fig. 47 shows the relation between the load and the tensile force in the steel beam for specimen C1 to C4 inclusive. The relation according to an elastic calculation for complete interaction (no slip) is indicated in the figure by the dashed line.

It appears from this figure that, in the beams C3 and C4, with degrees of shear connection of 49% and 27.5% respectively, the increase of the load is indeed overproportional to the increase of the tensile force in the steel beam.

For comparison the relation for test beam C5 is also given, which is practically identical to C4 but without prevention of the natural bond, as will be the case in practice. As slip is prevented by bond, the tensile force N_a initially increases more than in beam C4. However, after the bond has been broken, the tensile force remains almost constant with increasing load.

As the maximum tensile force in the steel beam is determined by the resistance of the shear connection, the relation between the ultimate load and the number of shear connectors (see Fig. 16) can also be derived from Fig. 47.

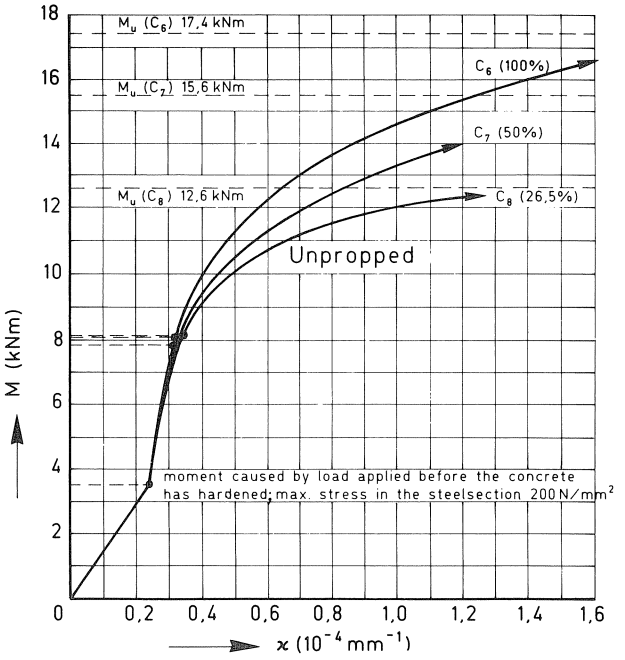

Fig. 43. Moment-curvature curves of test beams C6, C7 and C8.

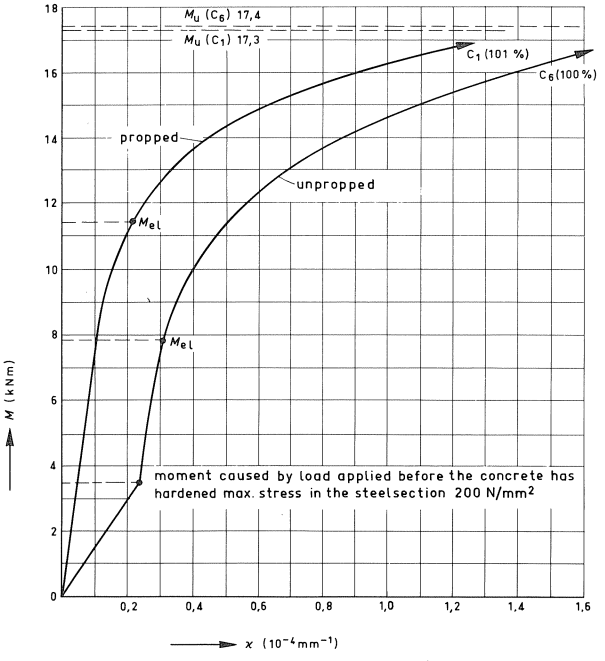

Fig. 44. Moment-curvature curves of test beams C1 and C6.

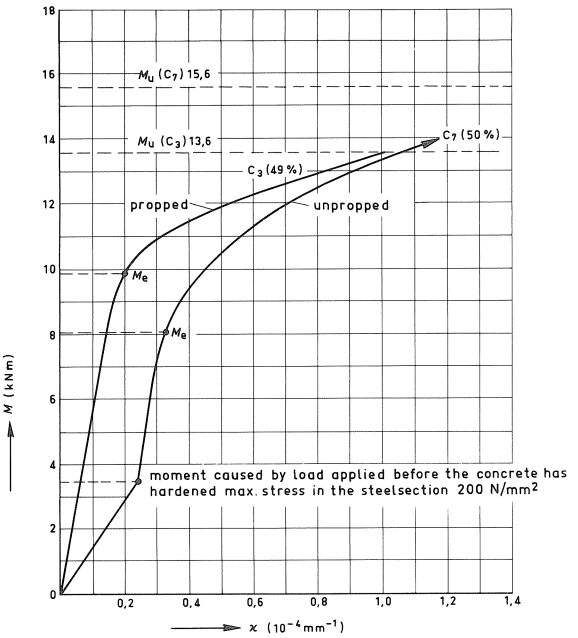

Fig. 45. Moment-curvature curves of test beams C3 and C7.

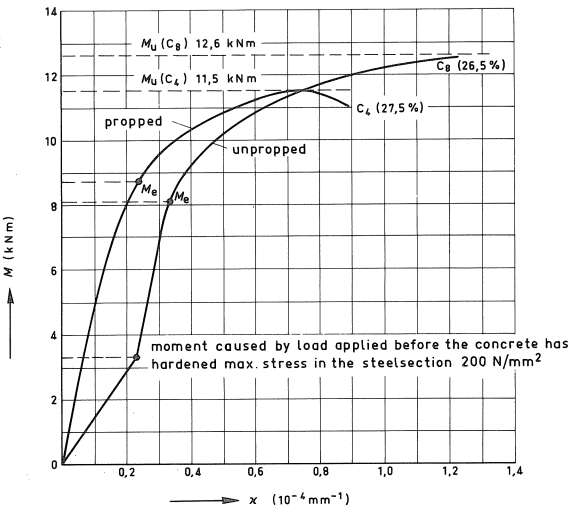

Fig. 46. Moment-curvature curves of test beams C4 and C8.

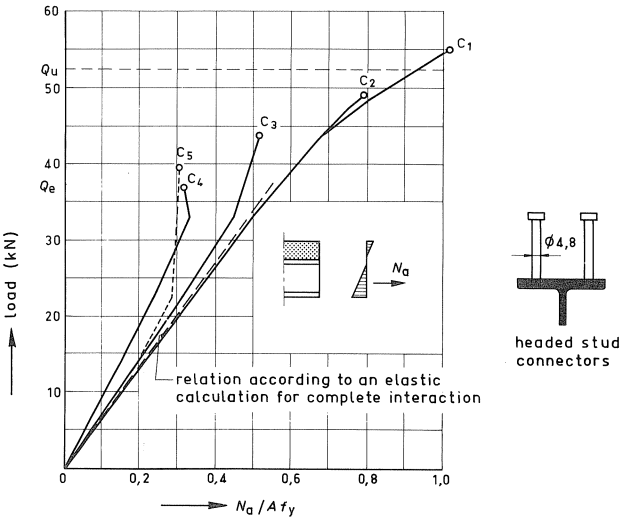

Fig. 47. Relation between the load and the tensile force in steel beam for the test beams with headed stud connectors (compare Fig. 16).

Fig. 48 shows the relation between the load and the tensile force in the steel beam (= load on the shear connectors) for the test beams with block-type shear connectors. Comparison with Fig. 47 shows that, with the same degree of shear connection, the ultimate load is smaller than the ultimate load of the test beams with headed stud connectors. The tensile force in the test beams D1, D2 and D3 follows almost exactly the qualitative relation for the absolutely rigid connection shown in Fig. 18. Only the beam with the smallest percentage of shear connectors (30%) behaves more favourably. The difference in behaviour is clearly shown in Fig. 49. In this figure the measured strains and stresses in the test beams of both series with a 30% and a 50% shear connection are compared.

The discontinuity in the strains at the interface between steel and concrete is considerably smaller in the test beams with block-type shear connectors than in the test beams with headed stud connectors. This lack of slip potential will cause the optimization of the stress distribution, as described for ductile shear connectors, to occur to a lesser extent or not at all.

The block type shear connectors were uniformly distributed over the shear span. From Fig. 48 the conclusion may be drawn from that the ductility of the block-type connectors was apparently sufficient to redistribute the forces over the shear connectors in such a way that at failure the forces on nearly all shear connectors were equal to their resistances. Indeed the tensile force in the steel beam at failure appeared to be equal to ΣS_{max}. Considering the relatively large difference between the theoretical and the experimental values of the maximum moments a considerable redistribution of stress could obviously occur in the test beams with the smallest degree of shear connection (D4 and D6, also see the line for D6 in Fig. 48).

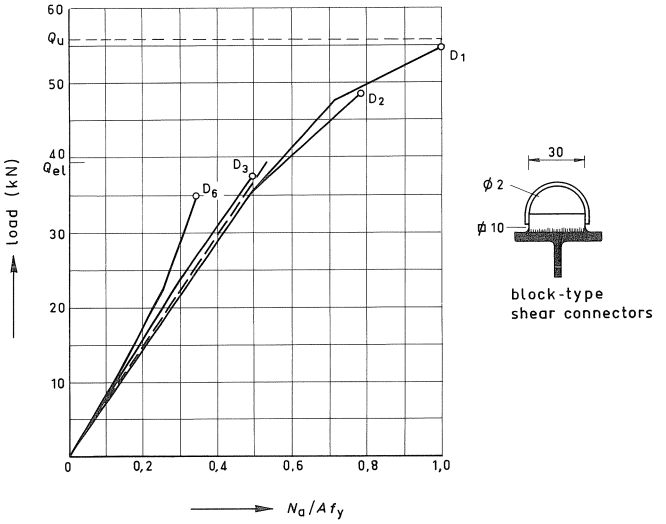

Fig. 48. Relation between the load and the tensile force in steel beam for the test beams with block-type shear connectors (compare Fig. 17).

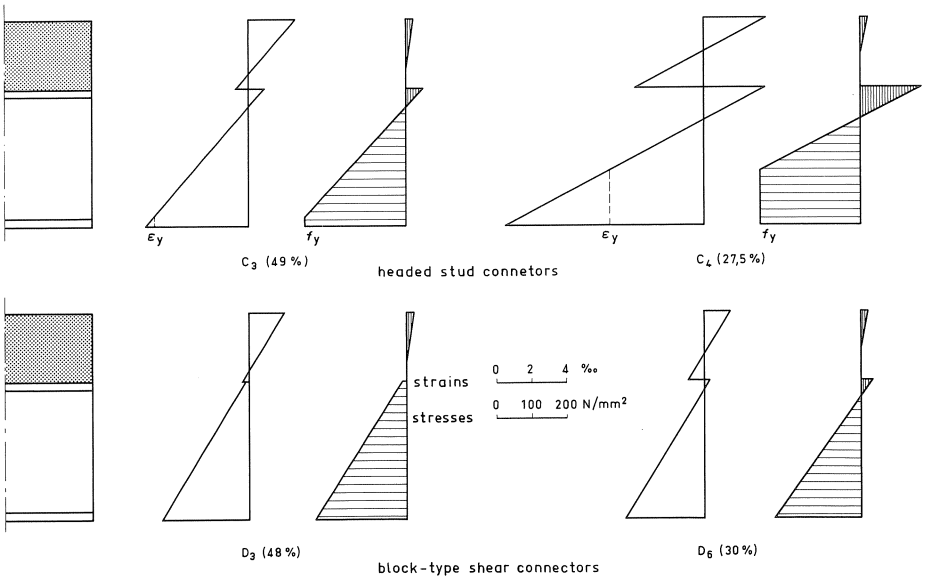

Fig. 49. Measured strains and stresses for load $F = 33$ kN.

4.2 *Tests on small-scale continuous beams*

In literature quite a lot of tests on continuous beams with full shear connection are described. These tests offer sufficient experimental evidence for the design methods discussed in chapter 2 for beams with full shear connection. On the other hand, when this research project was started, no useful information was available about tests on continuous beams with partial shear connection.
The importance of the possibility to a apply partial shear connection was discussed in chapter 1. The research was therefore focused on the development of a theoretical model and practical design rules for that type of beams. Apart from a theoretical approach, an experimental verification was considered necessary. So a test programme on small-scale beams was carried out. This test programme links up with the tests on small-scale simply supported beams as discussed in 4.1.

4.2.1 Test programme and material properties

The project included static loading tests up to failure on 11 beams.
The dimensions of the beams are given in Fig. 50. The dimensions of the cross-sections are identical to those in the tests on simply supported beams as discussed in 4.1. The test beams may be considered as models with a scale of about 1 : 3.
All beams were subjected to four concentrated loads per span, as is shown schematically in Fig. 51. This figure also shows the moment distribution in the elastic range and at failure.
Fig. 52 shows the test set-up.

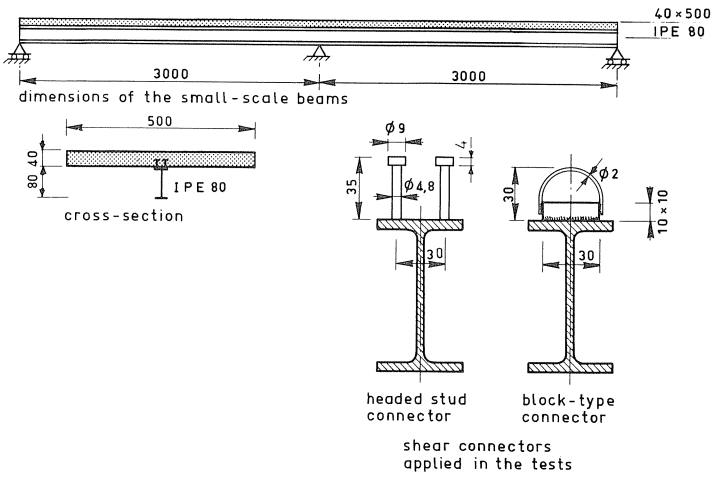

Fig. 50. Dimensions of the small-scale beams and the shear connectors used.

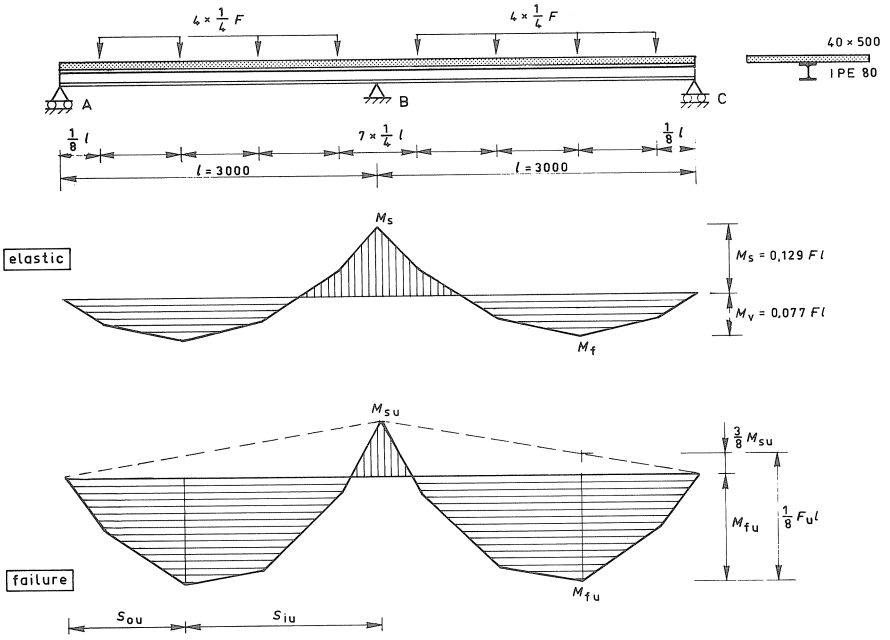

Fig. 51. Load arrangement and moment distribution.

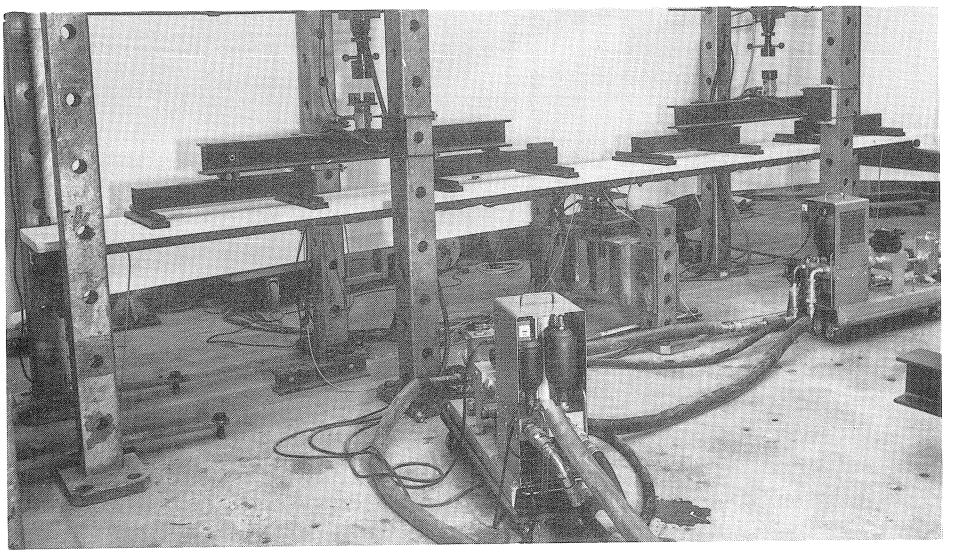

Fig. 52. The test set-up.

The influence of the following parameters was examined.

a. The number of shear connectors.
The main aim of the test programme was to verify the theoretical model for beams with partial shear connection. The number of shear connectors in the external span (S_{ou}) and the number of shear connectors in the internal span (S_{iu}) were varied. Table 4 shows the values of S_{ou} and S_{iu}. In brackets the degree of shear connection is given, defined as:

$$\frac{S_{ou}}{Af_y} \times 100\% \quad \text{and} \quad \frac{S_{iu}}{Af_y} \times 100\%$$

b. Distribution of the shear connectors.
In all tests the shear connectors in the external shear span were distributed uniformly. In the internal shear span the number of shear connectors in the sagging moment region and in the hogging moment region were chosen separately. The position of the point of contraflexure is determined for the moment distribution at failure and for full shear connection. In these two separate parts the shear connectors are distributed uniformly. Table 4 also shows the resistances of the shear connection in these separate parts.

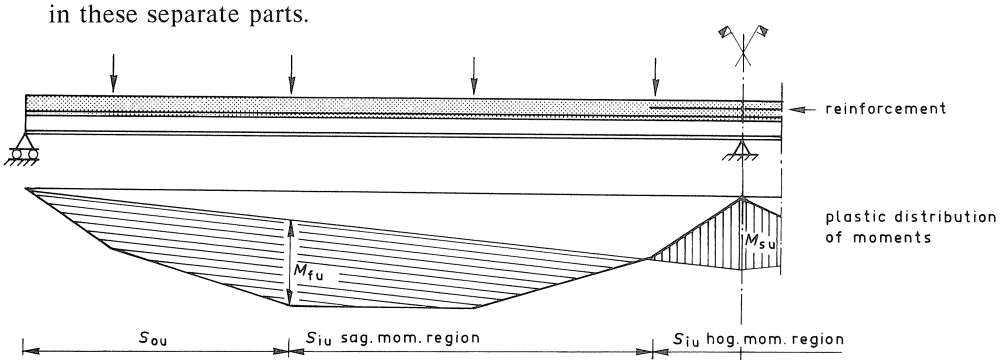

Table 4. Test programme

test beam	shear connector	cross-section reinforcement	resistance shear connection (kN (%))				distribution S_{iu} (kN)	
			S_{ou}		S_{iu}		sagging moment region	hogging moment region
FA 1	headed stud	254	255	(110)	391	(113)	255	136
FA 2	headed stud	254	255	(99)	280,5	(76)	255	25,5
FA 3	headed stud	254	255	(119)	153	(47)	127,5	25,5
FA 4	headed stud	254	127,5	(49)	161,5	(44)	127,5	34
FA 5	headed stud	254	255	(117)	0	(0)	0	0
FB 6	headed stud	99	255	(112)	306	(113)	255	51
FB 7	headed stud	99	255	(94)	272	(87)	255	17
FB 8	headed stud	99	127,5	(50)	144,5	(48)	127,5	17
SA 9	block-type	254	240	(104)	360	(105)	240	120
SA 10	block-type	254	240	(104)	168	(49)	120	48
SA 11	block-type	254	120	(53)	168	(50)	120	48

c. The amount of reinforcement.
Two different values were chosen for the amount of reinforcement A_s.
- A "heavy" reinforcement.
The yield strength of the reinforcement was taken roughly equal to half the yield strength of the steel section. The cross-section is then:

$$A_s = 0.5 \frac{Af_y}{f_{sy}}$$

Based on the specified material properties, this choice results in a value of 0.75 for the ratio M_{ssu}/M_{fsu}.
- A "light" reinforcement.
This was taken as 0.5% of the cross-section of the concrete slab:

$$A_s = 0.005 \cdot 40 \cdot 500 = 100 \text{ mm}^2$$

When this light reinforcement is applied, the ratio M_{ssu}/M_{fsu} is 0.6, based on the specified material properties.

d. Type of shear connector.
Just as in the tests on simply supported beams, the following two types of shear connectors were used:
- ductile shear connectors: ⌀ 4.8 mm;
- rigid shear connectors: block ⏍ 10 mm.

Table 4 shows the test programme. The relevant measured material properties are summarized in Table 5.

Table 5. Dimensions and material properties

	concrete slab*		steel beam**			reinforcement***			shear connectors		
test beam	f'_{ck} (N/mm²)	E'_c (kN/mm²)	f_y (N/mm²)	A (mm²)	Z_{pl} (mm³)	f_{ys} (N/mm²)	A_s (mm²)	y (mm)	S_{ou} number	S_{iu} number	S_{max} (kN
FA 1	36	28,5	297	784	23700	440	254	69,0	30	30 + 16	8,5
FA 2	36	28,5	336	765	23000	440	254	69,0	30	30 + 3	8,5
FA 3	36	28,5	280	764	23000	440	254	69,0	30	15 + 3	8,5
FA 4	36	28,5	339	764	23000	440	254	69,0	15	15 + 4	8,5
FA 5	36	28,5	285	764	23000	440	254	69,0	30	0	8,5
FB 6	37	29,0	297	764	23000	440	99	70,5	30	30 + 6	8,5
FB 7	37	29,0	354	764	23000	440	99	70,5	30	30 + 2	8,5
FB 8	37	29,0	336	764	23000	440	99	70,5	15	15 + 2	8,5
SA 9	38	28,5	300	768	23100	440	254	69,0	10	10 + 5	24,0
SA 10	38	28,5	305	756	22800	440	254	69,0	10	5 + 2	24,0
SA 11	38	28,5	300	758	22800	440	254	69,0	5	5 + 2	24,0

* The intended strength of the concrete was 35 N/mm².
** The grade of steel was specified as Fe 360, with an average yield strength of 280 N/mm².
*** The position of the reinforcement is given by the distance y between the centre of gravity of the steel bean and the centre of the reinforcement (see also Fig. 27).

4.2.2 Calculation of the small-scale beams

Based on the geometrical data and the material properties as summarized in Fig. 50 and Table 5, the ultimate load of the test beams was calculated with the theory described in the chapters 2 and 3. The calculated values of the ultimate load F_{tu} are summarized in Table 8. Comparison of the absolute values of F_{tu} is difficult because the material properties of the test beams differ considerably. Therefore, as a reference for all test beams, the value of the ultimate load F_{su} for full shear connection was also calculated. For the test beams with partial shear connection this value is given in brackets. The non-dimensional values F_{tu}/F_{su} are mutually comparable. For the test beams with headed stud connectors the table also includes the values of the ultimate loads F_{iu} and F_{du} determined according to the simplified method discussed in 3.2.2. For the test beams with partial shear connection and block type shear connectors F_{tu} is also calculated with the theoretical model of 3.2.1. As this method is not intended for beams with non-ductile shear connectors, the values have been put in brackets and are only given for comparison.

Test beams with full shear connection: FA 1, FB 6 and SA 9

$$M_{fu} = Af_y \left(m - \frac{Af_y}{1.6 b_e f'_c} \right) \qquad \text{Fig. 11/equation (2.1)}$$

$$M_{su} = yA_s f_{sy} + M_{pl,red} \qquad \text{Fig. 14/equation (2.3)}$$

$$F_u = \frac{8M_{fu} + 3M_{su}}{l} \qquad \text{Fig. 19/equation (3.4)}$$

Table 6. Values of M_{fu}, M_{su} and F_u for the test beams FA 1, FB 6 and SA 9

test beam	M_{fu} (kNm)	M_{su} (kNm)	F_u (kN)
FA 1	16,39	12,03	55,47
FB 6	15,98	9,58	52,20
SA 9	16,27	11,92	55,30

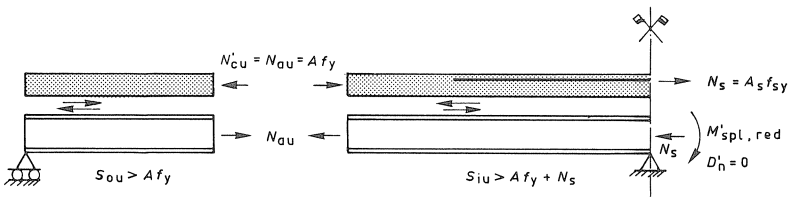

Fig. 53. Distribution of the forces in the test beams FA 1, FB 6 and SA 9.

Test beam FA 3 with $S_{ou} = 119\%$ and $S_{iu} = 47\%$

The ultimate load of this beam is first calculated with the assumption that $D'_n = 0$.

$$M_{su} = yN_s + M_{spl,red} = 11.34 \text{ kNm} \qquad \text{equation (3.11)}$$

$$M_{fu} = N'_{cu}\left(m - \frac{N'_{cu}}{1.6 b_e f'_c}\right) + M_{fpl,red}$$

$$= N'_{cu}\left(m - \frac{N'_{cu}}{1.6 b_e f'_c}\right) + 1.18 Z_{pl} f_y \left(1 - \frac{N'_{cu}}{A f_y}\right)$$

$$= 9.36 \text{ kNm} \qquad \text{equation (3.6)}$$

$$F_u = \frac{8M_{fu} + 3M_{su}}{l} = 36.29 \text{ kN} \qquad \text{equation (3.4)}$$

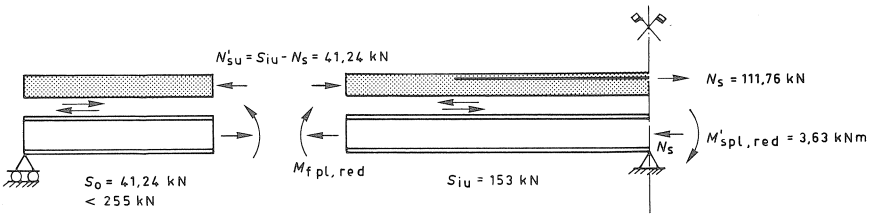

Fig. 54. Test beam FA 3 with $D'_n = 0$.

The optimum theoretical value is reached when $\bar{D}'_n = 143.85$ kN. Fig. 55 shows the corresponding distribution of forces at failure. The shear force S_0 is smaller than the resistance S_{ou}, so the shear plane in the external shear span is not critical. Striking is that a tensile force is working in the steel section over the internal support. This will be elaborated in the discussion of the test results. Based on the stress distribution shown in Fig. 55, the following values can be calculated:

$M_{su} = 7.51$ kNm
$M_{fu} = 14.35$ kNm
$F_{tu} = 45.78$ kN

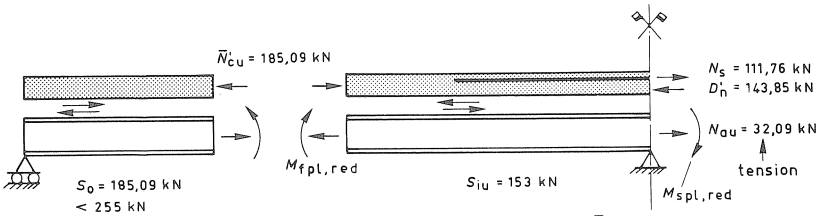

Fig. 55. Test beam FA 3 with $\bar{D}'_n$.

Test beam FA 4 with $S_{ou} = 49\%$ and $S_{iu} = 44\%$

A comparison of this beam with beam FA 3 is interesting since the optimum value of $\bar{D}'_n$ cannot develop because the shear plane in the external shear span becomes critical. This creates the possibility to directly calculate the maximum value of D'_n. For comparison with test beam FA 3 the calculation is first carried out with the assumption that $D'_n = 0$.

$$M_{su} = M_{ssu} = yN_s + M_{spl,red} = 12.94 \text{ kNm}$$

$$M_{fu} = N'_{cu}\left(m - \frac{N'_{cu}}{1.6 b_e f'_c}\right) + 1.18 Z_{pl} f_y \left(1 - \frac{N'_{cu}}{A f_y}\right) = 11.30 \text{ kNm}$$

$$F_u = \frac{8M_{fu} + 3M_{su}}{l} = 43.07 \text{ kN}$$

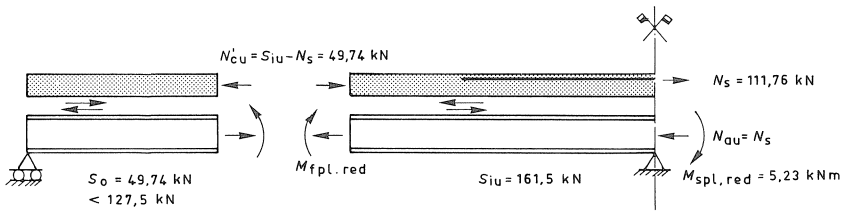

Fig. 56. Test beams FA 4 with $D'_n = 0$.

The optimum distribution of forces at failure is shown in Fig. 57. As the S_{ou}-plane is critical, the value of D'_n follows from:

$$D'_n = N_s + S_{ou} - S_{iu}$$

Based on this distribution of forces the following values can be calculated:

$$M_{su} = 12.14 \text{ kNm}$$
$$M_{fu} = 14.16 \text{ kNm}$$
$$F_{tu} = 49.89 \text{ kN}$$

Table 7. Determination of F_u for some values of D'_n.

D'_n (kN)	$N_{au} = -N_s + D'_n$ (kN)	$M_{spl,red}$ (kNm)	$M_{su} = N'_{au}y + D'_n y_0 + M_{spl,red}$ (kNm)	$N'_{cu} = D'_n + S_{iu} - N_s = D'_n + 41{,}25$ (kN)	$M_{fu} = N'_{cu}z + M_{fpl,red}$ (kNm)	F_u (kN)
0	−111,76	3,63	11,34 = 7,71 + 3,63	41,24	9,36 = 3,23 + 6,12	36,3
40	− 71,76	5,05	11,09 = 4,95 + 1,09 + 5,05	81,24	10,92 = 6,21 + 4,71	40,2
80	− 31,76	6,44	10,67 = 2,19 + 2,04 + 6,44	121,24	12,35 = 9,06 + 3,29	43,6
120	+ 8,24	6,44	8,73 = −0,57 + 2,86 + 6,44	161,24	13,65 = 11,78 + 1,87	45,1
160	+ 48,24	5,89	6,08 = −3,33 + 3,52 + 5,89	201,24	14,79 = 14,34 + 0,45	45,05
172,68	+ 60,92	5,44	4,95 = −4,20 + 3,71 + 5,44	$Af_y = 213{,}92$	15,14 = 15,14	45,03

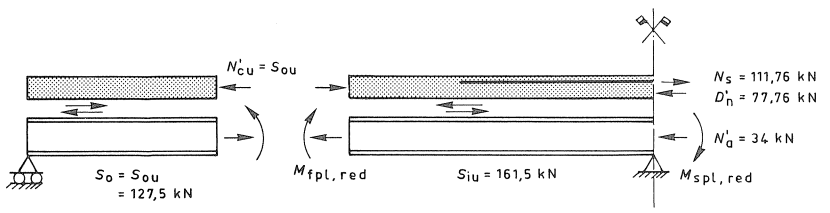

Fig. 57. Test beam FA 4 with optimum distribution of forces; the S_{ou}-plane is d critical.

Test beam FA 5 with $S_{ou} = 117\%$ and $S_{iu} = 0\%$

As appears from Fig. 58, this distribution of shear connectors does not allow for the assumption that $D'_n = 0$. For, when $D'_n = 0$, the equilibrium condition for the concrete slab in the internal shear span requires that N_s and N'_{cu} also have to be equal to zero (N'_{cu} compression only). The possibility of this very extreme shear connection is based on the development of D'_n. The sum of N_s and N'_{cu} is transferred over the support to the adjacent span. For the calculation of composite floors it has been suggested, on the basis of this predicted behaviour, to only use end anchorages in the end spans of continuous slabs. For that reason and also to be able to verify the theory in the extreme, it has been decided to include this test beam in the test programme. The distribution of the shear connectors, however, is far beyond the practical field of application. The optimum distribution of forces at failure is shown in Fig. 59. As was to be expected $S_0 \ll S_{ou}$, so the shear connection of the S_{ou}-plane is strongly overdimensioned. Based on this optimum distribution of forces the following values can be calculated:

$M_{su} = 0.95$ kNm
$M_{fu} = 11.96$ kNm
$F_u = 32.83$ kN

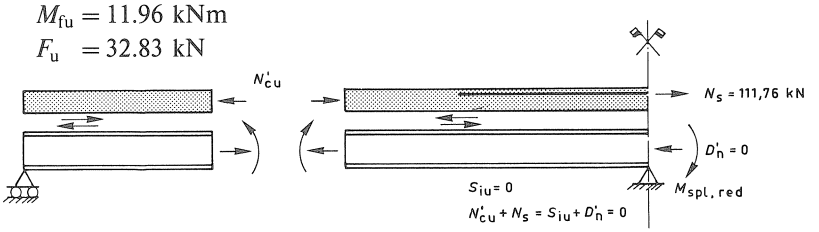

Fig. 58. Test beam FA 5 with $D'_n = 0$ is not possible.

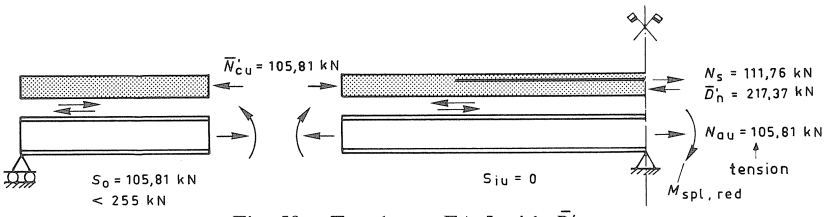

Fig. 59. Test beam FA 5 with $\bar{D}'_n$.

The normal force in the steel beam over the internal support is a large tensile force (compare test beam FA 3).

4.2.3 Test results and conclusions

Table 9 summarizes the measured values of the ultimate load F_{eu}. In view of the large differences in material properties of the various beams, the non-dimensional quantity $F_{eu}/F_{su} \times 100$ has also been calculated for easier mutual comparison. For comparison also the calculated results according to the theoretical model and the simplified methods F_{eu}/F_{tu}, F_{eu}/F_{iu} and F_{eu}/F_{du} respectively, are given. With the exception of test beam FA 2 and the test beams with block-type shear connectors, the correspondence

between the test results and the theoretical values is satisfactory. The experimental and theoretical results of the test beams with partial shear connection and block-type shear connectors differ considerably. This confirms that the theoretical model is only applicable if the shear connectors have sufficient deformation capacity. In test beam FA 2 a number of studs failed prematurely due to bad welds. Welding of the small-scale stud connectors appeared to be relatively sensitive to scatter of the material properties of the

Table 8. Calculated values of the ultimate load

			calculation results*				
test beam	S_{ou} (%)	S_{iu} (%)	F_{su} (kN)	F_{tu} (kN)	F_{tu}/F_{su} (·100%)	F_{iu} (kN)	F_{du} (kN)
FA 1	110	113	55,47	55,47	100	55,47	55,47
FA 2	99	76	(60,11)	58,74	97,7	52,49	53,92
FA 3	119	47	(51,72)	45,78	88,5	36,82	36,29
FA 4	49	44	(60,48)	49,89	82,5	42,62	43,07
FA 5	117	0	(52,48)	32,83	62,6	(24,04)	-
FB 6	112	113	52,20	52,20	100	52,20	52,20
FB 7	94	87	(60,60)	58,66	96,8	56,60	57,94
FB 8	50	48	(57,99)	47,28	81,5	42,57	45,78
SA 9	104	105	55,30	55,30	100	55,30	55,30
SA 10	104	49	(55,34)	(48,63)	(87,9)	-	-
SA 11	53	50	(54,70)	(45,52)	(83,2)	-	-

* F_{su} = the theoretical ultimate load for a full shear connection
F_{tu} = the theoretical ultimate load according to the theoretical model
F_{iu} = the calculation ultimate load with the interpolation method (see 3.2.3)

$$= F_{ou} + \frac{S_{iu}}{Af_y + A_s f_{sy}} (F_{su} - F_{ou})$$

F_{ou} = the ultimate load of steel beam
F_{du} = the calculated ultimate load with the assumption $D_n' = 0$ (see 3.2.3)

Table 9. Measured ultimate loads

			test results				
test beam	S_{du} (%)	S_{iu} (%)	F_{eu}** (kN)	F_{eu}/F_{su} (·100%)	F_{eu}/F_{tu} (kN)	F_{eu}/F_{iu} (kN)	F_{eu}/F_{du} (kN)
FA 1	110	113	60,00	108	1,09	1,08	1,08
FA 2*	99	76	51,79	86	0,88	0,99	0,96
FA 3	119	47	43,52	84	0,95	1,18	1,19
FA 4	49	44	50,71	84	1,02	1,19	1,18
FA 5	117	0	36,20	69	1,10	(1,50)	-
FB 6	112	113	50,20	96	0,96	0,96	0,96
FB 7	94	87	58,18	96	0,99	1,03	1,00
FB 8	50	48	46,73	81	0,99	1,10	1,02
SA 9	104	105	53,59	97	0,97	0,97	0,97
SA 10	104	49	36,48	66	(0,75)	-	-
SA 11	53	50	38,10	70	(0,84)	-	-

* in test beam FA 2 the studs failed prematurely
** F_{eu} = the measured load
For other notations see Table 8.

beam. Test beam FA 2 is one of the beams with an exceptionally high yield strength. This situation is not representative for the practice. However, the results of test beam FA 2 have been included for completeness. The ultimate loads calculated according to the two simplified methods are, as was to be expected, conservative compared to the test results.
Fig. 60 shows the load-deflection curves of the FA beams. The characteristic failure mode is indicated in the figure by a code. Fig. 63 contains some pictures to illustrate the failure modes. It is interesting to compare these results with the theoretical results (see Table 10).

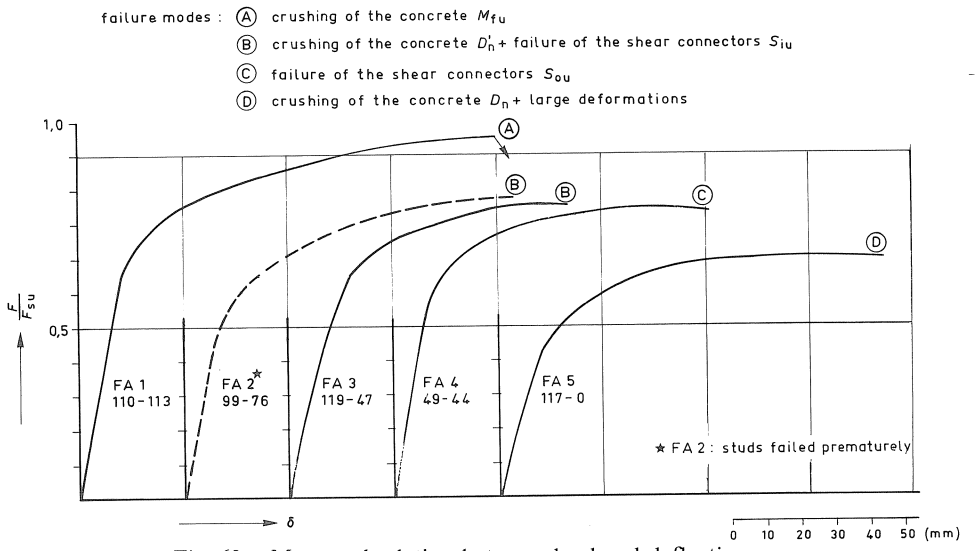

Fig. 60. Measured relation between load and deflection.

Test beam FA 1 (Fig. 53)
This is a beam with full shear connection. A mechanism develops with plastic hinges at M_{fu} and M_{su}. Continued rotation in the plastic hinge at M_{fu} causes the upper surface of the concrete slab to crush.

Test beam FA 3 (Fig. 55)
In this beam the shear plane S_{iu} is critical. At failure a large compressive force D'_n occurs at the internal support. This is clearly illustrated in Fig. 63b, which shows that the concrete of the underside of the concrete slab is crushed considerably above the internal support.

Test beam FA 4 (Fig. 57)
According to the calculation in beam FA 4 the S_{ou}-plane is critical. In the test considerable slip was indeed observed at the ends of the beam. This is illustrated in Fig. 63c.

Test beam FA 5 (Fig. 59)
This is a beam with a very extreme shear connection. As S_{iu} is equal to zero, the occurrence of a large compressive force D_n' is essential. This indeed occurred in the test. The deformations at failure were so large that the test had to be stopped before the maximum load was reached.

The theoretical model is supported by the failure modes as observed in the tests. The Figs. 61 and 62 show the load-deflection diagrams of the FB and the SA test beams. The FB beams show the same tendencies as the comparable FA beams, whereas the test beams with partial shear connection and block-type connectors differ. This is illustrated by a comparison of the beams SA 10 and SA 11 as shown in Fig. 62, with the beams FA 3 and FA 4 as shown in Fig. 60. Not only is the ultimate load of the SA beams con-

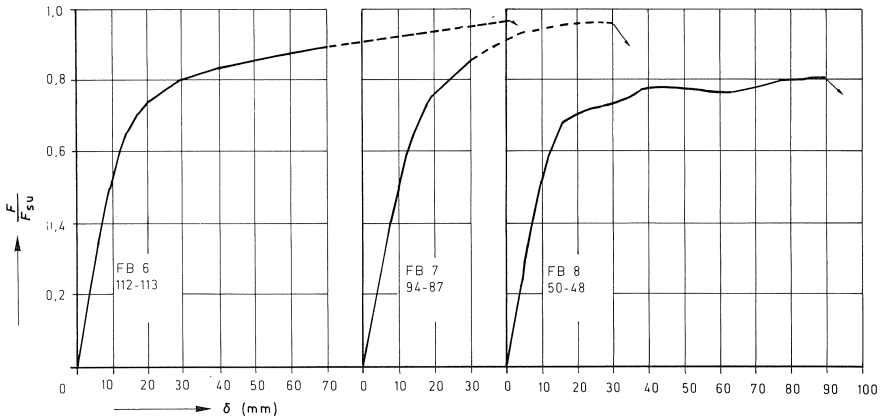

Fig. 61. Measured relation between load and deflection for test beams FB 6, FB 7 and FB 8.

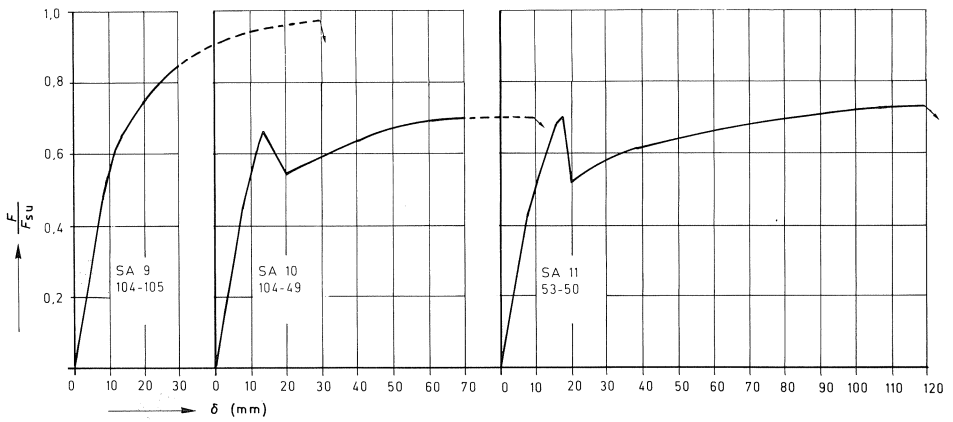

Fig. 62. Measured relation between load and deflection for test beams SA 9, SA 10 and SA 11.

siderably smaller, but the load also falls down drastically after relatively small deformations. Although the load can be increased after further deformation, this behaviour is undesirable for real structures.
In Table 10 the measured and calculated values of M_{fu} and M_{su} for the test beams with headed stud connectors are given. For completeness also the values of the ultimate load

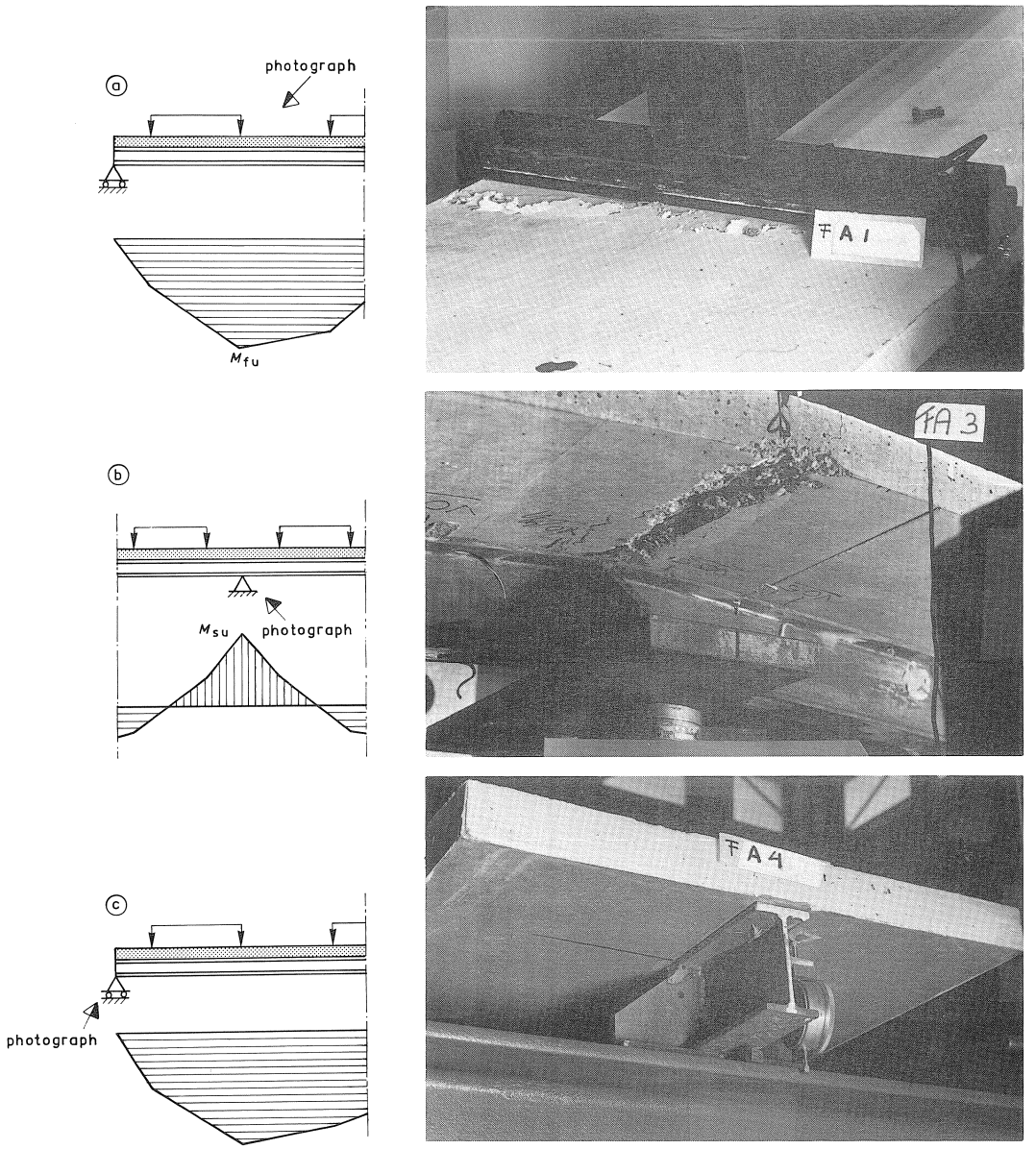

Fig. 63. Illustration of the failure modes.

Table 10. Measured and calculated values of M_{fu} and M_{su}

test beam	calculation			test			calculation result / test result		
	F_{tu} (kN)	M_{tfu} (kNm)	$-M_{tsu}$ (kNm)	F_{eu} (kN)	M_{efu} (kNm)	$-M_{esu}$ (kNm)	$\frac{F_{eu}}{F_{tu}}$	$\frac{M_{efu}}{M_{tfu}}$	$\frac{M_{esu}}{M_{tsu}}$
FA 1				60,00	19,3	8,4	1,08		
FA 2	55,47	16,3	12,0	55,50*	16,8	11,4	1,00	1,03	0,99
FA 3	45,78	14,3	7,5	43,52	13,9	7,9	0,95	0,97	1,09
FA 4	49,89	14,2	12,1	50,71	15,1	12,1	1,02	1,06	1,00
FA 5**	32,83	12,0	0,9	36,20	12,4	3,5	1,10	0,98	-
FB 6	52,20	16,0	9,6	50,20	16,6	7,7	0,96	1,04	0,83
FB 7	58,66	17,6	11,1	58,18	18,5	10,4	0,99	1,05	0,94
FB 8	47,28	14,1	9,7	46,73	14,8	7,6	0,99	1,05	0,78

* With this load M_{su} reaches its maximum.

** The distribution of forces at failure has not completely developed. The test was stopped because of large deformations.

are given in this table. The sagging moments of resistance (M_{fu}) generally seem to be somewhat higher than predicted by the theoretical model. On the other hand the hogging moments of resistance (M_{su}) are smaller. A deviation of M_{su} is not that serious, because the hogging moment is considerably smaller than the sagging moment and also because the contribution of M_{su} to the ultimate load is smaller, as follows from $F_u = 1/l(8M_{fu} + 3M_{su})$. This is confirmed by the satisfactory agreement between F_{eu} and F_{tu}. The normal force in the steel beam can be derived from the strains measured in 8 cross-sections. Fig. 64 shows the relation of the load and the normal force in the cross-sections 1 and 4 and 8 and 5 respectively. The results are given for the beams with partial shear connection, namely test beams FA 3, FA 4 and FA 5. The calculations of these beams were discussed before. As a reference also the results of test beam SA 9 are given, which has full shear connection with block-type connectors. It may be assumed that the results of beam SA 9 give the best approach to the theoretical case of complete interaction. Comparison of the results shown in Fig. 64 with the calculation leads to the following conclusions.

Test beam FA 3

With small values of F, section 4 close to the internal support (distance 130 mm), is subjected to a compressive force in the steel section. When the load increases over $F \approx 15$ kN this compressive force becomes smaller and changes its sign when approaching the ultimate load. This is caused by the increase of the compressive force $\bar{D}'_n$. It has to be noted that according to the calculation (see Fig. 55), the normal force in the steel beam over the internal support is also a tensile force.

The figure shows that the theoretical value of N_{au} in this test beam deviates considerably from the value observed in the test. It has to be kept in mind that the ultimate load F_u is not very sensitive to the magnitude of $N_{au} = N'_{cu}$, which is confirmed by Table 5.

Test beam FA 4

In this test beam the compressive force close to the internal support increases for a longer period than in test beam FA 3. This indicates that the compressive force D_n' develops later. The tensile force in section 5 at failure is smaller than in test beam FA 3. This indicates that the value of D_n' will also be smaller. This is in agreement with the calculation. Compare Figs. 57 and 55. It has to be kept in mind that the points of measurement 4 and 5 are some distance away from the internal support.

Test beam FA 5

In this test beam with an extreme moment distribution, it is essential that a compressive force D_n' develops from the start. Fig. 64 shows that the normal force in the steel beam in cross-section 4 is, also with a small load, already a tensile force. This tensile force increases progressively with increasing load. Also in the calculation (see Fig. 59) a large tensile force was observed in the steel beam. So the tendency of the course of the normal forces is in agreement with the theoretical model. For the absolute magnitude of N_{au} a remark identical to the one made for test beam FA 3 is valid.

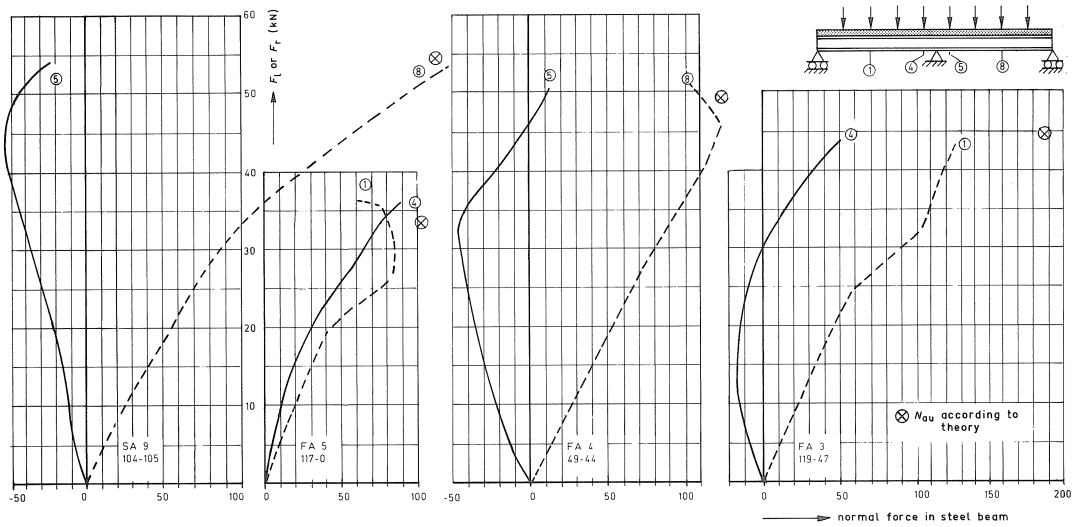

Fig. 64. Relation between the load and the normal force in the steel beam.

5 Summary

In this publication the theoretical and experimental results of a research project on the behaviour of composite beams with partial shear connection are presented.
Partial shear connection is an important option for the economic use of composite beams in buildings. It enables the designer to use a smaller number of shear connectors

in cases where it is not feasible or necessary to provide as many shear connectors as required for full shear connection. This gives the designer the possibility to choose between a light steel beam with relatively more shear connectors and a heavier steel beam with fewer shear connectors. Apart from this economical comparison, partial shear connection will always be advantageous when an oversize steel beam must be selected from the available rolled beam size, or when deflection controls and strength requirements are met by less than full composite action. Partial shear connection may even be a "must" when a profiled steel sheet is used as formwork for the concrete slab. The size and spacing of the ribs can dictate the maximum number of connectors that can be placed.

The first contribution to the development of a theory for the ultimate strength of beams with partial shear connection was presented by Slutter and Driscoll in 1965. They suggested that the resistance of the cross-section of the beam can be determined on the basis of a rigid-plastic stress distribution (rectangular stress blocks) for normal forces in the slab and the beam equal to the total resistance of the shear connectors in the relevant shear span. It is self-evident that the shear connectors must be able to deform sufficiently for this stress distribution to develop.

To investigate the influence of the deformation capacity of the shear connectors a test programme was carried out in the Netherlands by TNO-IBBC. A number of small-scale simply supported beams with headed stud connectors as well as block-type connectors was tested. The results were confronted with a partial connection theory. This work was published in Dutch in 1971 [7] and [8]. The research has shown both theoretically and experimentally that the deformation capacity of connectors has a significant influence on the resistance of beams with partial shear connection. A simplified design method was proposed for both ductile and rigid non-ductile connectors. The simplified method was included in the Dutch Recommendations and also in the European Model Code.

Later a similar research programme was carried out on continuous composite beams. The theoretical model based on rigid-plastic material behaviour, as proposed by Slutter and Driscoll, was extended to continuous beams and verified by a series of small-scale tests. This work was published in Dutch in 1987 [2]. Because this subject is again under discussion during the preparation of Eurocode 4, it was decided to publish the results of both the research programmes on simply supported beams and continuous beams in English in this edition of Heron.

6 Notations

A cross-section area of steel beam
A_s cross-section area of reinforcement
A_{st} cross-section area of reinforcement in top of concrete slab
A_{sb} cross-section area of reinforcement in bottom of concrete slab
b_e effective width of the concrete slab
D'_n compressive force in the lower part of the concrete slab at the internal support
ε_a strain in steel

ε_{at} strain in the top fibre of the steel beam
ε'_c strain in concrete
ε'_{cu} ultimate strain in concrete
ε_y strain in steel at yield strength
E_a modulus of elasticity of steel
E'_c modulus of elasticity of concrete
f'_c compressive strength of concrete
f'_{ck} characteristic compressive strength of concrete
f_y yield strength of structural steel
f_{sy} yield strength of reinforcing steel
F_{du} calculated ultimate load with the assumption that $D'_n = 0$
F_{eu} measured ultimate load
F_g load during construction, before steel and concrete act compositely
F_{iu} ultimate load calculated with the interpolation method
F_{ou} ultimate load of the steel beam
F_{su} theoretical ultimate load for a full shear connection
F_{tu} ultimate load according to the theoretical model
F_u ultimate load
h_t total height of the composite beam
h_s height of the concrete slab
h'_s reduced height of the concrete slab (distance between the bottom surface of the top reinforcement and the bottom surface of the concrete slab)
l span length of the composite beam
m distance between upper side of the concrete slab and centre of the steel beam
M_e maximum elastic moment of resistance (first yield in extreme fibre)
M_{el} elastic moment of the steel beam
M_{pl} plastic moment of the steel beam
$M_{pl,red}$ reduced plastic bending moment of the steel beam
M_{fu} hogging moment of resistance
M_{fsu} hogging moment of resistance in case of a full shear connection
M_{su} sagging moment of resistance
M_{ssu} sagging moment of resistance in case of a full shear connection
M_u moment of resistance
n number of shear connectors
N_a tensile force in the steel beam
N_{au} ultimate tensile strength of the steel beam
N'_{au} ultimate compressive strength of the steel beam
N'_c compressive force in the concrete slab
N'_{cu} ultimate compressive strength of the concrete slab
N_e tensile force in the steel section belonging to the moment M_e
N_{fsu} tensile force in the steel section belonging to the moment M_{fsu}
N_s tensile strength of the reinforcement
σ_a steel stress

σ'_c concrete stress
S longitudinal shear force
S_a longitudinal shear force in a cantilever part
S_{au} longitudinal shear resistance of a cantilever part
S_i longitudinal shear force in an internal shear span
S_{iu} longitudinal shear resistance of an internal shear span
S_o longitudinal shear force in an external shear span
S_{ou} longitudinal shear resistance of an external shear span
S_u longitudinal shear resistance
V longitudinal shear force in the beam
V_u longitudinal shear resistance of the beam
x height of the compressive zone of the concrete
y lever arm between a tensile force in the reinforcement and a compressive force in the steel beam (hogging moment sections)
y_0 lever arm between a tensile force in the reinforcement and a compressive force in the lower part of the concrete slab (hogging moment sections)
z lever arm between a compressive force in the concrete slab and a tensile force in the steel beam (sagging moment sections)
Z_{pl} plastic section modulus
Z_{el} elastic section modulus

7 Literature

1. CUR/SG rapport 1, Statisch bepaalde staal-beton liggers: theorie en richtlijnen, Delft, september 1974.
2. CUR/SG rapport 4, Statisch onbepaalde staal-beton liggers: theorie en richtlijnen, Delft, juli 1987.
3. Eurocode 2, Design of concrete structures Part 1 - General rules and rules for buildings, final draft, december 1988.
4. Eurocode 3, Design of steel structures Part 1 - General rules and rules for buildings, edited draft, 1989.
5. Eurocode 4, Composite steel and concrete structures, first draft, oktober 1984.
6. NEN 3851, TGB Staal, Nederlands Normalisatie Instituut, 1972.
7. Stark, J. W. B., Over de berekening van vrij opgelegde samengestelde liggers met volledig schuifsterke verbinding, TNO-IBBC rapport BI-71-51, Rijswijk, 1971.
8. Stark, J. W. B. and H. E. Brassinga, Liggerproeven op verkleinde schaal, TNO-IBBC rapport BI-71-52, Rijswijk, 1971.